Biomedicine & Pharmacotherapy 159 (2023) 114262

Contents lists available at ScienceDirect

Biomedicine & Pharmacotherapy

journal homepage: www.elsevier.com/locate/biopha

Fighting secondary triple-negative breast cancer in cerebellum: A powerful aid from a medicinal mushrooms blend

Fabrizio De Luca [a,1], Elisa Roda [b,1], Daniela Ratto [a], Anthea Desiderio [c], Maria Teresa Venuti [a], Martino Ramieri [a], Maria Grazia Bottone [a], Elena Savino [c], Paola Rossi [a,*]

[a] Department of Biology and Biotechnology "L. Spallanzani", University of Pavia, 27100 Pavia, Italy
[b] Laboratory of Clinical & Experimental Toxicology, Pavia Poison Centre, National Toxicology Information Centre, Toxicology Unit, Istituti Clinici Scientifici Maugeri IRCCS, 27100 Pavia, Italy
[c] Department of Earth and Environmental Science, University of Pavia, 27100 Pavia, Italy

ARTICLE INFO

Keywords:
TNBC
Cerebellum
Medicinal mushrooms
Metastases
Locomotor activity
Cancer proliferation
Apoptosis
Integrative medicine

ABSTRACT

Breast cancer (BC) is the second most common cause of brain metastasis onset in patients, with the cerebellum accounting for the 33% of cases. In the current study, using a 4T1 triple-negative mouse BC model, we revealed that an orally administered medicinal mushrooms (MM) blend, rich in β-glucans, played a direct and specific anti-cancer action on cerebellar metastases, also bettering locomotor performances. The neuroprotective effect of the MM blend plays through (i) a direct and specific inhibition of cerebellar metastatization pattern typical of TNBC (with an induced reduction of about 50% of metastases density) and (ii) the regulation of apoptosis and proliferation-related genes, as suggested by expression changes of specific molecular markers, i.e. PCNA, p53, Bcl2, BAX, CASP9, CASP3, Hsp70 and AIF. Therefore, inhibiting the metastatization process, triggering a significant apoptosis increase, and lessening cell proliferation, this MM supplement, employed as adjuvant treatment in association with conventional therapy, could represent a promising approach, in the field of Integrative Oncology, for patients' management in both prevention and treatment of brain metastases from BC.

1. Introduction

Female breast cancer (BC) is the most commonly diagnosed cancer worldwide, with an incidence of 2,261,419 cases and mortality of 684,996 individuals in 2020 [1]. BC is a heterogeneous disease, showing a tumour phenotype characterized by peculiar histological and metastatic features, as well as different therapeutic response and clinical outcome [2,3]. Nowadays, 5 clinical subtypes of BC have been identified, based on their gene expression profile or biomarkers expression [4]. Among these tumours, approximately 10–20% are triple-negative breast cancer (TNBC), testing negative for estrogenic and progesterone receptors, and for the epidermal growth factor receptor 2 (HER2). TNBC is the most aggressive BC, with either high proliferation or metastatic phenomena, high rate of recurrence, often associated with poor prognosis, and unresponsiveness to current targeted therapies [5–7].

Metastatic colonization in TBNC involves cellular and molecular processes, which act to stimulate angiogenesis and tumour-stroma interactions, as well as intravasation through the basement membrane with subsequent extravasation into the distant target organs [8]. Actually, BC is the second most common cause of brain metastasis onset. In particular, Central nervous system (CNS) is the first metastatic target in 12% of BC patients, being also detected in 30% of autopsy series [9–11].

Abbreviations: BC, Breast Cancer; TNBC, Triple-Negative Breast Cancer; HER2, Human Epidermal growth factor Receptor 2; CNS, Central Nervous System; BMBC, Brain Metastases from BC; BBB, Blood Brain Barrier; MM, medicinal mushrooms; BRMs, Biological response modifiers; MU-care, Micotherapy U-care; TME, Tumor Microenvironment; PCNA, Proliferating Cell Nuclear Antigen; Bcl-2, B-cell lymphoma 2; BAX, Bcl2 Associated X; CASP9, Caspase 9; CASP3, Caspase 3; Hsp70, 70 kDa Heat shock protein; PBS, Phosphate-Buffer Saline; QoL, Quality of Life; H&E, Hematoxylin and Eosin; PSR, Picrosirius Red; OD, Optical Density; IGL, Internal Granular Layer; PCs, Purkinje cells; WM, White matter; ML, Molecular layer; AIF, Apoptosis-inducing factor.

* Corresponding author.
E-mail addresses: fabrizio.deluca01@universitadipavia.it (F. De Luca), elisa.roda@icsmaugeri.it (E. Roda), daniela.ratto01@universitadipavia.it (D. Ratto), anthea.desiderio01@universitadipavia.it (A. Desiderio), mariateresa.venuti01@universitadipavia.it (M.T. Venuti), martino.ramieri01@universitadipavia.it (M. Ramieri), mariagrazia.bottone@unipv.it (M.G. Bottone), elena.savino@unipv.it (E. Savino), paola.rossi@unipv.it (P. Rossi).
[1] These authors have contributed equally to this work and share first authorship.

https://doi.org/10.1016/j.biopha.2023.114262
Received 14 November 2022; Received in revised form 5 January 2023; Accepted 14 January 2023
Available online 17 January 2023

During the last 40 years an increase in the onset of brain metastases from BC (BMBC) has been perceived, possibly due to the discovery and use of novel therapies, which result in longer patient survival, as well as to advances in neuroimaging allowing a punctual detection of early metastases [12,13]. Notably, among the different regions of CNS, cerebellum is the main site of metastases occurrence accounting for the 33% of cases, together with basal ganglia, [14–16]. This preferential location is probably ascribable to the high blood supply of this area [17] and to a "leaky" blood brain barrier (BBB) that allows the passage of metastatic cells into the CNS [17,18], a process characterized by a close cross-talk between the microenvironment and the tumour cells [19].

Currently, the standard of care consists of chemotherapy in case of BMBC, although with reduced efficacy due to the presence BBB, which limits the efficacy of chemotherapic drugs to reach the CNS. Alternative conventional therapeutic approaches, resulting in longer patients' survival, include surgery, whole-brain radiation and stereotactic radiosurgery. Nevertheless, the lack of an effective targeted therapy and the TNBC heterogeneity emphasized the urgent need to identify new therapeutic targets and develop novel effective medicines capable to overcome drug resistance.

One of the most promising sources of "drug discovery" in cancer adjuvant therapy are medicinal mushrooms (MM), which possess a long story of use in traditional oriental medicine mainly in China and Asia, also employed as nutritionally functional foods. A bulk of literature clearly evidenced that MM own peculiar anticancer, onco-immunological, and immunomodulatory properties, also improving quality of life during conventional oncological treatment protocols in humans [20,21].

Indeed, in the last years, the use of several MM has been approved as adjuvant supplements in antitumor therapy in different countries. Different MM produce hundreds of bioactive compounds which are able to influence, often in a synergistic way, numerous cancer-related pathways, modulating cellular targets typically involved in cell proliferation, survival, and angiogenesis [21,22]. In particular, anticarcinogenic, antimutagenic, onco-immunological and immunomodulatory effects in BC are closely linked to the type and amount of β1–3 and β1–6 glucans and to their modulation of the innate and cell-mediated immune response [7,23]. Such compounds act as biological response modifiers (BRMs), stimulating the immune system and consequently helping on cancer fighting. In fact, β-glucans are recognized by dectin-1 receptors by antigen presenting cells, thus "training innate immunity", which results in enhanced host reaction. This trained immunity holds great potential for boosting immune responses in frail subjects, i.e. oncological patients, and even some of these fungal β-glucans are already under evaluation on clinical trials [24–27].

Numerous literature data evidenced that the use of MM extracts or their compounds is secure and helpful when employed alone or even combined with conventional anticancer treatments [21,22].

One of the cellular mechanism that is involved in cancer is the evasion of apoptosis which results in therapy resistance [28]. Furthermore, inefficient apoptotic pathway activation and proliferation are two combined mechanisms leading to further cancer progression and metastatization. New apoptosis-targeted agents developed in breast cancer, such as Bcl2-inhibitors, are in front line and are undergoing clinical trials and other are needed as a new way to treat cancer [28].

Our previous studies employing a syngeneic mouse of 4T1 triple-negative BC demonstrated the striking beneficial effects of an oral supplementation with "Micotherapy U-care" (MU-care), a MM blend, containing a combination of extracts of mycelia and sporophores. In particular, we proved that three month-lasting MU-Care supplementation ameliorated murine quality of life and contextually led to a remarkable decrease of metastases density and nodules number in pulmonary district, paralleled by a substantial decrease of inflammation and oxidative stress in metastases [7,29]. Moreover, we revealed that MU-Care was efficacious to influence cell death/proliferation balance, being these mechanisms strictly joined and inversely associated. Hence, our findings highlighted that MM blend owns a direct effect on tumour cells compelling cancer cells to apoptosis.

Recently, the same MM blend was employed for cancer patients' management after the failure of conventional treatment; specifically, MU-care has been administered in four subjects suffering from different tumour types, including breast cancer, with an improvement of survival and quality of life [30].

Herein, we evaluated the effect of MU-care in the before reported experimental conditions, using the 4T1 triple-negative mouse BC model, focusing on cerebellum. In particular, we addressed distinctive endpoints relative to cell death pathway also exploring pathological outcomes of the murine cerebellar tissue, comparing metastatic areas and neighbouring Purkinje cells. Specifically, cerebellar histopathology was investigated, together with the immunohistochemical assessment of key molecules, i.e., PCNA, p53, Bcl2, BAX, CASP9, CASP3, Hsp70 and AIF. Parallelly, locomotor performances were examined in vivo, being the cerebellum critically implicated in the control of motor behavior over cortical regions via cerebello-thalamic-cortical loops, also playing a pivotal role in balance and locomotion. In particular, we intended to evaluate possible functional changes due to damages in the cerebellar circuits [29–32].

Using a comparative approach, overall results were evaluated with the final goal to assess whether MU-care could exert beneficial effects also on CNS secondary breast cancer.

2. Results

As previously described [7] using the same preclinical model, i.e. the 4T1 triple-negative mouse BC, we demonstrated that MU-Care supplementation was accompanied by a betterment of QoL. Among selected parameters, we analyzed locomotor performances, demonstrating an astonishingly improvement of locomotor capabilities of treated mice, paralleled by a striking beneficial effect in pulmonary tissue [7].

In current investigation, we focused on the MU-care supplementation effect on the cerebellum, the main metastatic target area in BMBC patients. Therefore, functional measures of locomotor performances were complemented by histopathological characterization and immunohistochemical data about the expression of specific biomarkers representative of proliferation/cell death pathway in treated and not treated syngeneic mice compared to healthy control animals.

2.1. MU-care supplementation increased locomotor activities

We monitored locomotor parameters of mice before and after 4T1 cells injections in treated and not treated mice. In a variant of the open-field test, mice were left to explore freely an open and safety environment for eight minutes. We measured three locomotor parameters, i.e. the total distance, the mean speed, and the resting time. Specifically, open arena test was performed in treated mice (i) before starting MU-care treatment and prior to the tumor injection, namely "pre" condition (experimental time T1), and (ii) 20 days after 4T1 cells inoculation (T2). In untreated mice open arena test were performed (i) prior to the tumor injection, namely "pre" condition, and (ii) 20 days after 4T1 cells inoculation, namely "post" condition, in which pre and post represent T1 and T2, respectively.

Notably, concerning untreated mice only, all the examined parameters were similar pre- and post-4T1 injection, while the MU-care supplementation significantly improved locomotor performances (Fig. 1 A, B, C and Table 1). In particular, in untreated mice the total distance Fig. 1A), the mean speed Fig. 1B), and the resting time Fig. 1C) recorded "pre" and "post" were comparable. Any statistically significant difference was measured between "pre" and "post" condition in untreated mice and "pre" condition in the treated experimental group.

MU-care supplementation significantly enhanced murine locomotor activities despite 4T1 cells injection, as evidenced by a 57.2% increase in total distance Fig. 1A), a 22.2% increment in mean speed Fig. 1B) and a

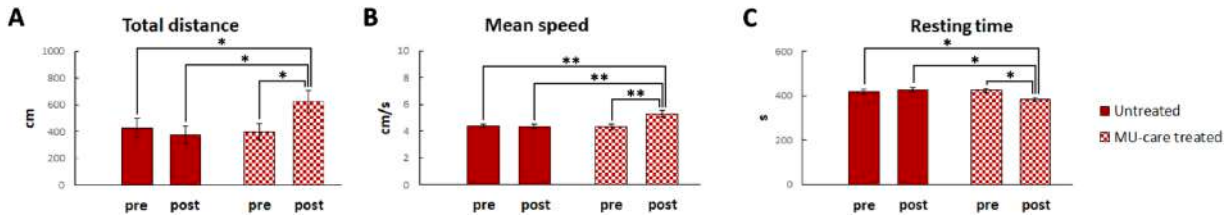

Fig. 1. Locomotor activity measured before (pre) and after (post) 4T1 cell injections in Untreated (red) and MU-care treated (blue) mice. A: Total distance (cm). B: Mean speed (cm/s). C: Resting time (s). $p < 0.05$ (*) and $p < 0.01$ (**) was calculated by One-way Anova followed by Bonferroni's post hoc test.

Table 1
Quantitative measurement of selected parameters, i.e. total distance (cm), mean speed (cm/s) and resting time (s), for studying locomotor performances before (pre) and after (post) 4T1 cell injections in Untreated and MU-care treated mice.

	Total distance (cm)		Mean Speed (cm/s)		Resting time (s)	
	pre	*post*	*pre*	*post*	*pre*	*post*
Untreated	425.07 ± 70.35	373.15 ± 66.66	4.36 ± 0.13	4.33 ± 0.15	417.14 ± 10.96	427.14 ± 9.57
MU-care treated	397.42 ± 59.67	624.82 ± 83.41	4.32 ± 0.17	5.28 ± 0.27	424.74 ± 9.07	384.19 ± 9.24

9.5% decrease in resting time Fig. 1C).

2.2. Cerebellar metastases density reduction in syngeneic mice by MU-care blend

Cerebellar vermes (sagittal sections) were processed to evaluate injury extent in cerebellar cortex comparing healthy controls, untreated, and MU-care treated mice by H&E, Nissl and PSR staining. All evaluations were performed focusing the attention on both cortical and bottom areas of cerebellar lobules.

Morphological picture obtained by H&E and Nissl staining in healthy controls (**a**), MU-care treated (**b-c**) and Untreated (**d-f**) mice are illustrated in Fig. 2. Healthy controls displayed a physiological cerebellar cytoarchitecture. Diversely, both Untreated and MU-care treated mice displayed the presence of a similar amount of micrometastases, localized in the entire thickness of cerebellar cortex, (Fig. 2, Panel H and Table 2).

Furthermore, in the same experimental groups, metastases were identified, mainly located within the internal granular layer (IGL) thickness and in the white matter (WM). These pathological formations were frequently surrounded by hemorrhagic foci scattered in the deep portions of the cerebellar lobules. Strikingly, the successive quantitative analyses revealed a statistically significant reduction (about 50%) in the number of deep WM cerebellar metastases after MU-care supplementation (Fig. 2, Panel I and Table 2). Focusing on the different cell types of cerebellar cortex layers, any morphological change was perceived in the three experimental groups.

Therefore, based on the significant metastases' density difference between Untreated and MU-care treated mice, we focused our attention on metastases.

2.3. Effect of MU-care on collagen staining in syngeneic mice

Results acquired after PSR cerebellum staining in healthy controls (a, d), and MU-care treated (b, c) and Untreated (e, f) mice are depicted in Fig. 3. This staining allows the study of collagen networks in normal and pathological paraffin-embedded tissues. The PSR labeling was mainly evident both at meningeal level as well as in the IGL cells in all experimental groups. In particular, a statistically extremely significant increase of PSR OD was measured in the meninges of Untreated mice compared to healthy controls. Remarkably, in MU-care treated animals the measured OD fell between the two aforementioned values, being therefore significantly different compared to that determined both in Untreated mice and healthy controls, (Fig. 3, Panel H and Table 2). Otherwise, concerning the PSR OD assessed at IGL cells level, any significant difference was established among the three experimental groups (Fig. 3, Panel I and Table 2). Concerning metastatic areas, although no quantifiable collagen-positivity was detectable in the cerebellar metastases, PSR staining enabled an easier identification of metastatic tissue, evidencing the occurrence of surrounding hemorrhaging foci engulfed by yellow-labeled erythrocytes.

2.4. MU-care neuroprotection affecting proliferation/cell death imbalance in cerebellar metastases of syngeneic mice

The persistence of inflammation and oxidative state can lead to extensive cell and tissue damage over time. As adaptive response to injury, cells can trigger several defense mechanisms such as increasing antioxidant enzyme levels or activating programmed cell death pathways. The following sections report the data obtained investigating precise molecules, as specific markers of cell death pathways with the goal to explore the occurrence of such hypothesized adaptive mechanism.

The maintenance of a balance between proliferation and cell death is crucial for physiological cells and tissues homeostasis. **PCNA** is one of the key molecules involved in DNA replication, as a nuclear proliferation marker typically overexpressed in cancer cells. PCNA immunopositivity was detected at metastatic level (Fig. 4). The quantitative analysis revealed an extremely statistically significant increase in the number of immunoreactive metastatic cells OD (Fig. 4, **Panel I** and Table 3) and, with a similar trend, an extremely statistically significant enhancement of immunopositive cell density was detected in the metastatic areas of Untreated animals compared to MU-care treated mice (Fig. 4, **Panel H** and Table 3).

p53 is one of the most studied transcription regulators molecules and a tumor suppressor factor which regulates a wide range of genes involved in countless cellular functions, ranging from the DNA repair mechanisms to cell cycle regulation as well as to cell death mechanisms, i.e. apoptosis and autophagy, being these latter two critical points in cancer [33]. Our current data demonstrated that p53 immunoreactivity was mainly localized in the IGL both in MU-care treated and Untreated animals (Fig. 5). The presence of some p53-immunopositive micrometastases was also observed in the IGL of MU-care treated mice. Concerning metastases, a scarce number of p53-immunopositive cells were present, while an extremely significant increase of p53 immunopositive cells OD was detected comparing MU-care treated and Untreated mice (Fig. 5, **Panel H** and Table 3).

Bcl2 protein is a well-known anti-apoptotic factor. In the present study, Bcl2 immunoreactivity was mainly localized at PCs level in all experimental groups and also in metastatic areas (Fig. 6). Notably, focusing on metastases, a slight decrease was measured in metastatic cell density comparing MU-care treated and Untreated animals (Fig. 6, **Panel H** and Table 4). Interestingly, concerning metastases OD, a very significant immunopositivity decrease was perceived in MU-care treated mice compared to Untreated animals () (Fig. 6, **Panel I** and Table 4).

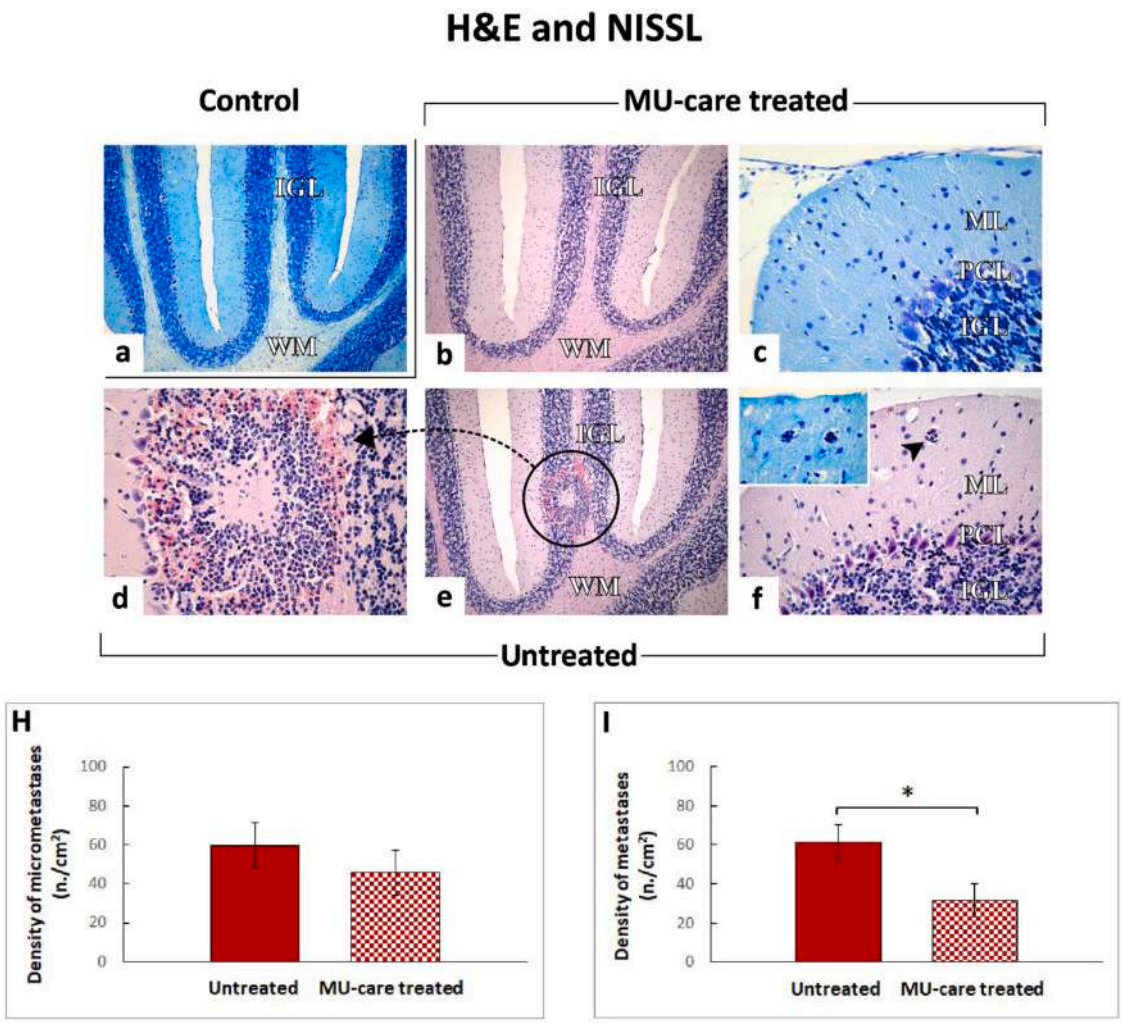

Fig. 2. Histological characterization by H&E and Nissl staining. Representative serial cerebellar vermis sections, showing parenchyma and metastatic areas (both macro- and micro-metastases), from healthy control (**a**), MU-care treated (**b, c**), and Untreated (**d–f**) mice. The physiological cerebellar structure appeared well preserved in healthy controls (**a**). Peculiar structural alterations evident in cerebellar parenchyma are presented, together with different metastatic features, in both MU-care treated and Untreated mice. ML: Molecular layer; PCL; Purkinje cells layer; IGL: Internal granular layer; WM: White matter. Circle and dotted arrow: deep metastasis identified in WM. Arrowhead: micro-metastasis localized in ML. Light microscopy magnification: 10x (**a, b** and **e**); 40 × (**c, d** and **f**); 60 × (insert in **f**). **Panels H** and **I**: Histograms showing quantification of micrometastases and metastases density, respectively. *p* value calculated by unpaired Student's t-test: (*) < 0.05.

Table 2
Quantitative assessment of (i) metastases and micrometastases density by H&E and NISSL staining and (ii) Meninges and IGL cells OD by PSR staining. —: *not present.*

	H&E and NISSL		Picrosirius Red	
	Density of micrometastases	*Density of metastases*	*Meninges OD*	*IGL cells OD*
Control Untreated	—	—	75.80 ± 2.80	55.80 ± 0.93
MU-care treated	59.52 ± 11.64	61.22 ± 9.24	101.06 ± 3.09	57.05 ± 1.15
	45.63 ± 11.52	31.74 ± 8.46	90.62 ± 3.11	58.72 ± 1.04

Concerning the pro-apoptotic molecule **BAX**, its expression was particularly manifest at metastatic level in all synergic tumor-bearing mice, both Untreated and MU-care treated (Fig. 7). In detail, an extremely statistically significant enhancement of both immunopositive cells OD and density were measured in MU-care treated mice compared to those determined in Untreated animals (Fig. 7**, Panel H and I,** and Table 4). Notably, in the same experimental groups, at parenchyma level the immunoreactivity was not measurable, similarly to the situation observed in healthy controls.

CASP9 is the most well-studied initiator caspase, playing a key role in the mitochondrial or intrinsic pathway. In particular, CASP9 immunolabeling was primarily detected at PCs soma level as well as in the metastases (Fig. 8). In particular, as regards to metastases, an extremely significant increase of immunopositive cell density was assessed in MU-care treated mice compared to Untreated (Fig. 8**, Panel H** and Table 5). Similarly, an extremely significant augment of immunopositive cells OD was measured in MU-care treated mice compared to Untreated animals (Fig. 8**, Panel I** and Table 5).

CASP3 is one of the effector molecules triggering apoptosis (Fig. 9). A slight augment was determined evaluating metastases cell density in MU-care treated compared to Untreated animals). (Fig. 9**, Panel I** and Table 5). Likewise, a slight increase of CASP3 immunopositive cells OD was measured in MU-care treated mice compared to Untreated animals (). (Fig. 9**, Panel J** and Table 5).

As a chaperone protein, **Hsp70** is chiefly involved in inhibiting apoptosis. Hsp70 immunostaining was mainly observed at PCs level (both soma and main dendrites) in all experimental groups, and also in

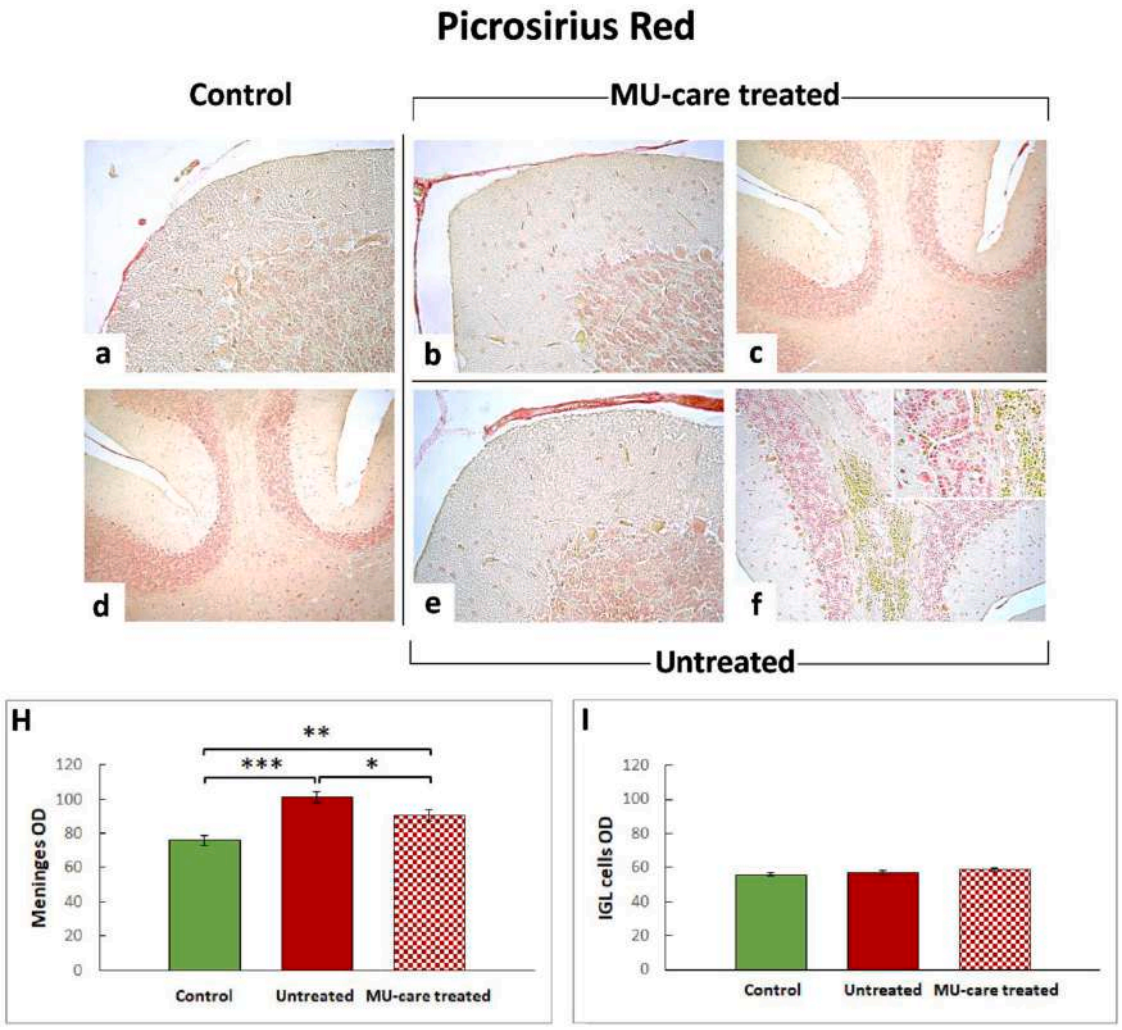

Fig. 3. Bright-field PSR staining. Representative cerebellar specimens, showing parenchyma and metastasis, from healthy control (a, d), MU-care treated (b, c), and Untreated (e, f) mice. Intensely labeled meninges were observable in Untreated mice (e). A weaker PSR OD positivity was detected in the IGL of healthy controls (a, d), MU-care treated (b, c), and Untreated (e, f) mice. The presence of a hemorrhagic core, engulfed with PSR yellow-labeled erythrocytes, surrounding unstained metastatic cells, was also evident (f). Light microscopy magnification: 10x (c and d); 20x (f); 40 × (a, b and e; insert in f). Panel H and I: Quantification of meninges and IGL cells OD, respectively. *p* values calculated by one-way ANOVA followed by Bonferroni's post-hoc test: (*) < 0.05; (**) < 0.01; (***) < 0.001.

metastatic areas in 4T1 injected mice (Fig. 10). (Fig. 10**, Panel H and I,** and Table 6). Notably, Hsp70 immunopositive cell density was generally extremely elevated in cerebellar metastatic tissues. In particular, Untreated mice displayed a significantly higher Hsp70 immunopositive cell density compared to MU-care treated animals (Fig. 10**, Panel H and I** and Table 6) Parallelly, concerning Hsp70 immunopositive cells OD, a significant lessening was measured comparing MU-care treated and untreated mice (Fig. 10**, Panel H** and **I and** Table 6).

2.5. MU-care parthanatos induction in cerebellar metastases of syngeneic mice

Parthanatos is a cell death mechanism which differs from all other known types of cell death, e.g. apoptosis or necrosis. This multistep cell death pathway plays a key role in tumorigenesis and includes several critical molecules involved in tumor progression, invasion and metastatization. **AIF** is one of the main molecules involved in parthanatos and the translocation of this factor from the cytoplasm to the nucleus is a critical event in this cell death [34]. Results obtained after AIF immunohistochemistry in healthy controls (**a**), MU-care treated (**b - d**) and Untreated (**e – i**) mice are reported in Fig. 11 **and** Table 6. The AIF labeling was mainly evident in ML and metastatic tissue of both MU-care treated (**c, d**) and Untreated (**g, i**) mice, as well as in the IGL of Untreated animals only (**e**). Focusing on metastatic regions, a slight increase of AIF immunopositive cell density was observed comparing MU-care treated and Untreated animals (Fig. 11**, Panel J** and Table 6). Showing a similar trend, a significant increase of AIF immunopositive cell OD was measured in metastases of MU-care treated mice compared to the Untreated animals (Fig. 11**, Panel K** and Table 6).

3. Discussion

MU-care is a MM blend rich in β-glucans. In the current study, using a syngeneic tumour-bearing mouse of TNBC, we explored the MU-care effects on secondary breast cancer in cerebellum. We previously described, in the same animal model, MU-care beneficial action on lung metastases and in mice QoL. MM and their main active constituents β-glucans are known for their anticancer, anti-inflammatory and immunomodulatory properties both in vitro and in vivo [35–37] Few available papers focused on MM-derived β-glucans effects on brain cancer in vivo [26]. In the present study, we describe, for the first time, the in vivo effect of a MM blend rich in β-glucans on cerebellar secondary breast cancer in a triple negative syngeneic mouse. Notably, any other therapy was associated with MU-care during experimental time,

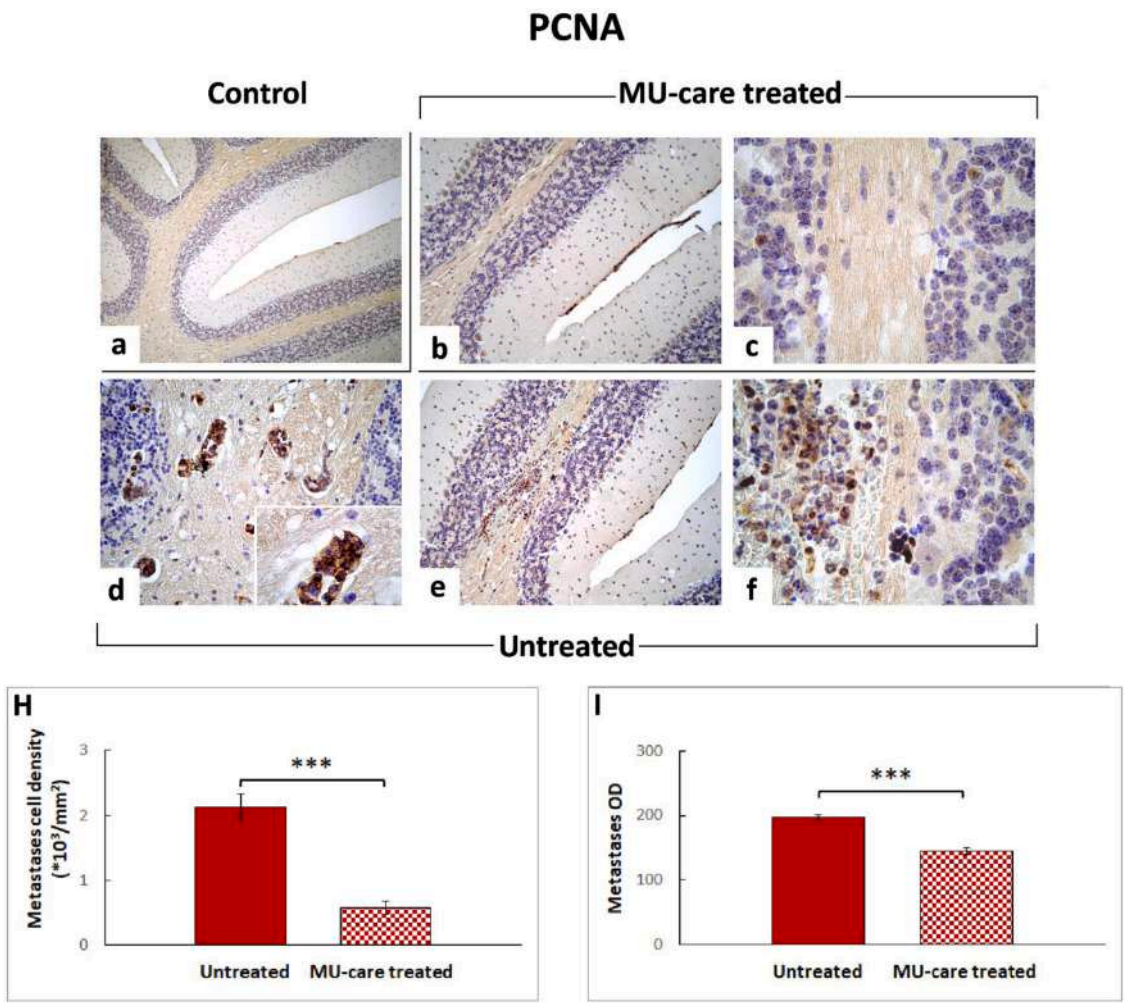

Fig. 4. Immunohistochemical labelling for PCNA in healthy control (a), MU-care treated (b, c), and Untreated (d–f) mice. A marked PCNA immunopositivity was evident mainly at metastatic level, more intense in Untreated (f) mice compared to MU-care treated (c). A strong immunolabeling was also visible in the deep WM of Untreated mice only (d). Light microscopy magnification: 10 × (a); 20 × (b, e); 40 × (d); 60 × (c, f, insert in d). Panels H and I: Histograms illustrating the quantitative assessment of immunoreactive metastases cell density and OD, respectively. *p* value calculated by unpaired Student's t-test: (***) < 0.001.

Table 3
Quantitative measurement of key proliferation/suppression molecules, namely PCNA and p53, in metastases. n.c.: not comparable.

	PCNA		P53	
	Cell density	OD	Cell density	*OD*
Untreated	2.13 ± 0.20	196.90 ± 4.14	n.c.	112.27 ± 1.99
MU-care treated	0.58 ± 0.10	144.49 ± 4.52	n.c.	139.21 ± 1.67

therefore we assumed that all described effects could be ascribable to the preventive and therapeutic (namely, effective during supplementation) effect of the MM blend.

In our experimental design, the syngeneic tumour-bearing mice were supplemented starting two months before 4T1 injection and lasting for an additional 35 days during tumour development, employing the MU-care drink, consisting of a mixture of five MM species, and characterized by a high 1,3–1,6 β-glucans content [7].

Through behavioural test experiments to assess locomotor activity, we revealed that supplemented mice, after 4T1 injection, were more active compared to untreated animals. Cerebellum is known to mediate sensorimotor adaptation, fine movement and coordination control, as well as instrumental conditioning [38–40]; hence, different behavioural tests could be conducted in lab animals. Nonetheless, it has to be highlighted that only a spontaneous behavioural test, namely open arena test, was chosen in our study, due to physiological BALB/c mice characteristics, e.g. high anxiety-like behaviour and limited exploratory performance [41,42]. All the tested locomotor parameters, i.e., the mean speed, the total distance, and the resting time, demonstrated a significant improvement in locomotor performances in MU-care mice. For fairness, it has to be mentioned that we cannot completely ruled out that the improvement of the locomotor activity could be attributable to MM beneficial effect on other brain regions and/or on muscular system, but the cerebellar metastatic areas observed in untreated mice tends to suggest a possible decline in their cerebellar network function. Remarkable, MU-care supplementation significantly increased the murine mean speed, a parameter analogous to the gait speed in humans. Gait speed is an important measure of functional status and health, since the ability to walk is one of the basic everyday activities [43–45], but it is a complex task that requires higher cognitive processes [46]. In particular, gait is related to and supported by cerebellar functions [47] and cerebellar volume loss was recorded in patients with decline in memory and gait speed [48,49]. Indeed, it is known that the cerebellum plays a fundamental role in gait and motor functioning, as demonstrated by poor gait in patients with cerebellar ataxia [48,50] and also by neuroimaging studies confirming the cerebellar involvement in

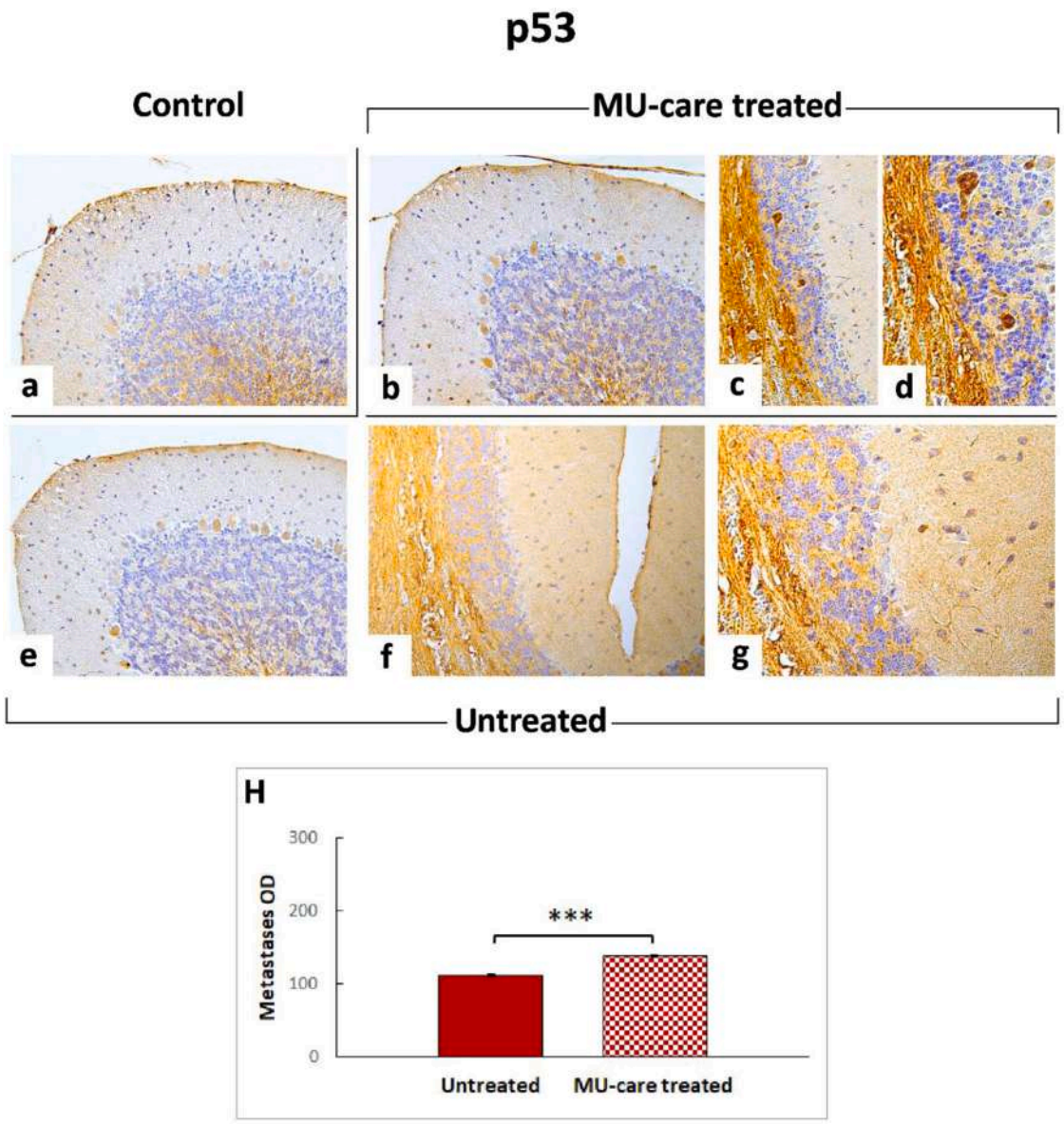

Fig. 5. Representative micrographs showing p53 immunohistochemical reaction in healthy control (**a**), MU-care treated (**b-d**), and Untreated (**e-g**) mice. An intensely marked p53 immunopositivity was observable particularly in micrometastases of MU-care treated mice (**c, d**); in these animals, metastases were also evidently immunoreactive (**c, d**). In Untreated mice, immunoposivity was clearly detected in metastatic areas (**f, g**). Light microscopy magnification: 40 × (**a, b, c, e, f**); 60 × (**d, g**). **Panel H**: histogram illustrating the quantitative analysis of immunopositive metastases OD. *p* values calculated by unpaired Student's t-test: (*) < 0.05, (**) < 0.01, (***) < 0.001.

sensorimotor coordination [51,52].

Histological, histochemical and immunohistochemical analyses in cerebellum were devoted to examine potential pathological features, in terms of cytoarchitectural alterations (with attention to different cerebellar cortex layers and cell types) and occurrence/number/extension of metastases.

H&E, having stood the test of time as the standard stain for histologic examination of tissues, enabling the recognition of different cells types and morphological changes, still remains the basis of contemporary cancer diagnosis [53,54].

In the current study, data obtained by means of H&E and Nissl techniques let us to highlight strong alterations in cerebellum of 4T1 tumour-bearing mice. In particular, the occurrence of several micrometastases and deep metastases was revealed, both in Untreated and in MU-care treated animals. This outcome fully matched with previous literature demonstrating that cerebellum is a typical metastatic site in BC patients [55]. These cerebellar neoformations were scattered both in WM as well as in ML of 4T1-injected mice. Notably, focusing on WM deep metastases, it has to be underlined that MU-care supplementation triggered a strikingly significant reduction in their number (about 50%). This data suggests that MU-care directly and specifically inhibit cerebellar metastasis of TNBC. Metastases were typically surrounded by haemorrhagic foci, appearing engulfed by yellow-labelled erythrocytes. It has also to be reported that, concerning the other different cell types of cerebellar cortex, any significant morphological alteration was observed neither in Untreated nor in MU-care treated animals.

Regarding collagen detection, PSR staining represents one of the most selective technique to identify and quantitatively estimate collagen deposition in histological sections. Fibrosis, resulting from chronic inflammatory process, is caused by an imbalance between collagen deposition and reabsorption. Tissue collagen quantification represents an important tool in the clinical diagnosis as well as for patients' outcome prediction and therapy individualization [56]. In the present investigation, PSR staining revealed a significant increase in collagen

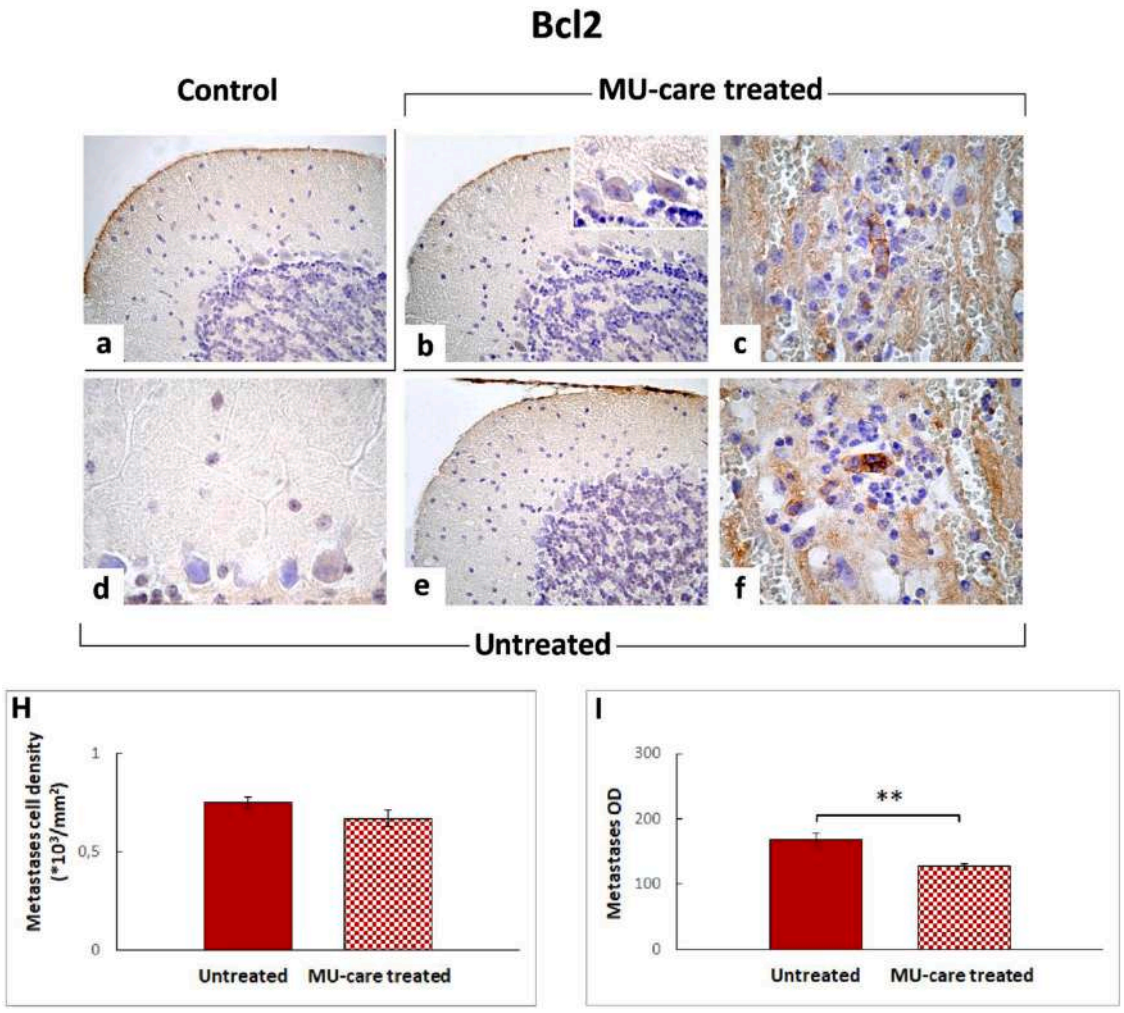

Fig. 6. Representative micrographs showing Bcl2 immunohistochemical reaction in healthy control (**a**), MU-care treated (**b, c**), and Untreated (**d–f**) mice. An intensely marked Bcl2 immunopositivity was observable particularly in PCs soma of MU-care treated mice (**b**); in these animals, metastases were also evidently immunoreactive (**c**). In Untreated mice, immunopositivity was detected in metastatic areas (**f**). Light microscopy magnification: 40 × (**a, b, e**); 60 × (**c, d, f**). **Panel H** and **I**: histograms illustrating the quantitative analysis of immunopositive metastases cell density and OD, respectively. *p* value calculated by unpaired Student's t-test: (**) < 0.01.

Table 4
Quantitative appraisal of crucial pro- and anti-apoptotic factors, namely Bcl2 and BAX, in cerebellar metastases.

	Bcl2		BAX	
	Cell density	*OD*	*Cell density*	*OD*
Untreated	0.75 ± 0.03	168.01 ± 9.84	0.39 ± 0.04	120.99 ± 6.75
MU-care treated	0.67 ± 0.04	127.23 ± 4.14	0.74 ± 0.05	168.37 ± 5.04

expression level in the meninges of 4T1-injected animals, with the Untreated mice resulting the most affected. In fact, cerebellar fibrosis tended to be reduced after MU-care supplementation. It has to be mentioned that, even though no quantifiable collagen-positivity was perceived in cerebellar metastases, Picric Acid itself enabled an easier recognition of deep metastases, highlighting the presence of yellow-labelled erythrocytes constituting haemorrhaging foci.

Based on our previous findings [7,29,57], we putatively assumed that MM blend could determine an imbalance between proliferation and cell death, driving to a significant increase in apoptotic event in metastatic tissue.

To test our hypothesis, we firstly assessed PCNA expression pattern after MM blend supplementation. In detail, a selective effect on the reduction of proliferation in cerebellar metastatic areas was evidenced in MU-care treated mice compared to untreated mice. Consequently, we postulated a protective role played by MM extract in DNA replication mechanism, and a direct and specific inhibitory effect on cancer cell proliferation.

Subsequently, we investigated the effect of MU-care on different apoptotic pathways. Initially, we examined Bcl2 immunohistochemical expression pattern [58–60]. Based on our data, we supposed that the lower Bcl-2 OD levels measured in cerebellar metastases of MU-care treated mice could be related to an imbalance between proliferation and apoptosis. Concerning cerebellar parenchyma (namely, PCs), Bcl-2 expression levels were comparable both in Untreated as well as in MU-care treated mice, thus suggesting a selective and specific apoptotic effect triggered by MM blend on metastases only.

Our aforementioned postulate was further reinforced by results obtained investigating BAX and p53. In particular, BAX, predominantly detected at metastatic level, displayed the highest expression levels in MU-care treated mice. This significant increase appeared to be in line with the well-known role of BAX, which acts as a proapoptotic protein. Thus, we could assume that an enhancement in BAX levels after MM supplementation could trigger tumour suppression. In accordance with our results, literature data demonstrated that, conversely, a decreased

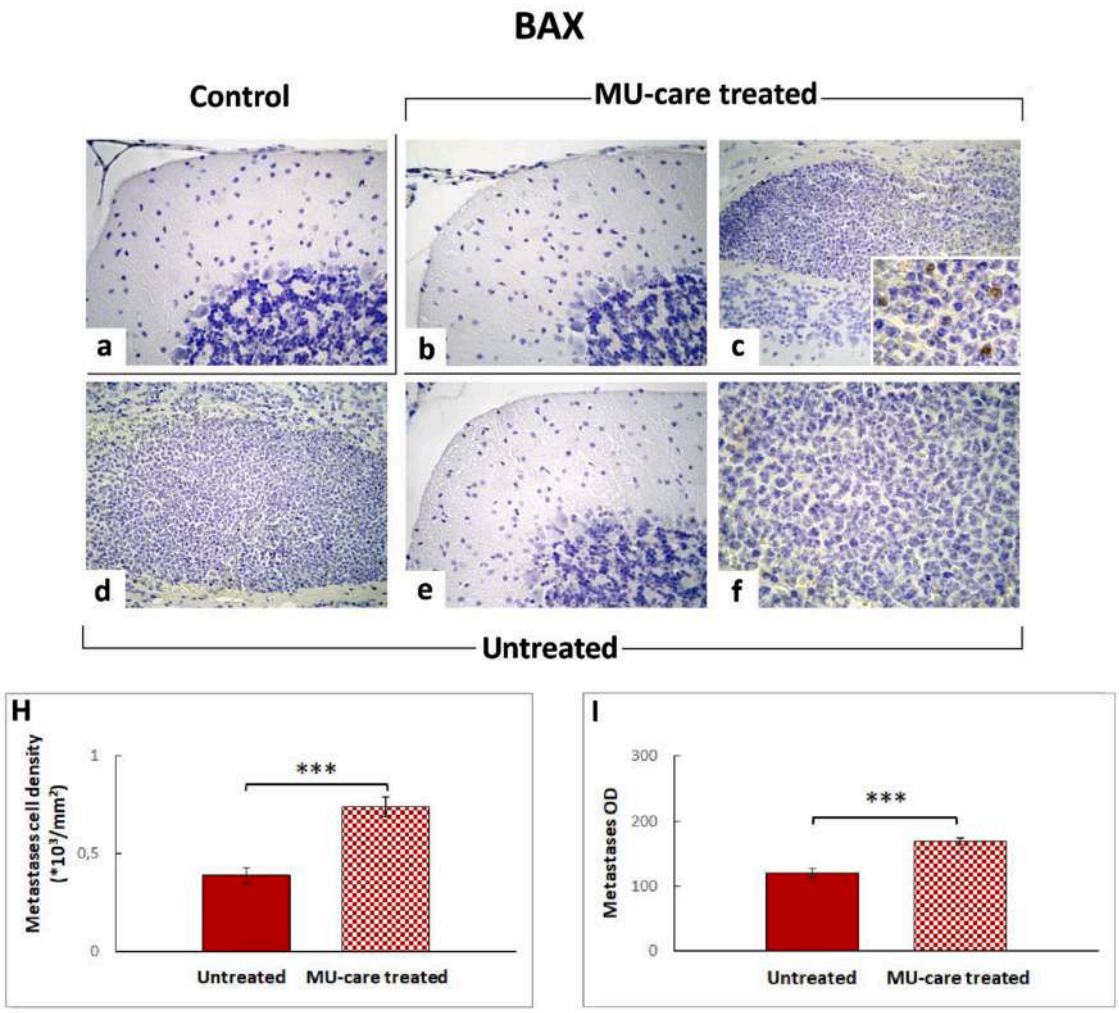

Fig. 7. Immunohistochemical labelling for BAX in healthy control (**a**), MU-care treated (**b, c**), and Untreated (**d–f**) mice. An intensely marked BAX immunoreactivity was clearly evident in metastatic areas of MU-care treated mice (**c**). Light microscopy magnification: 40 × (**a, b, c, d, e**); 60 × (**f**, insert in **c**). **Panels H** and **I**: Histograms showing the quantitative analysis of immunopositive metastases OD and cell density, respectively. *p* value calculated by unpaired Student's t-test: (***) < 0.001.

BAX expression would provide tumour cells with a selective survival advantage, contributing to their expansion and invasion [58]. Showing a similar trend, p53 exhibited the most marked increase in metastatic regions of MU-care treated mice. This enhanced immunopositivity for the wild type p53 isoform (wtp53), playing a crucial role deciding whether DNA would be repaired or the damaged cell would self-destruct, could indicate a possible attempt to cell cycle arrest, in order to inhibit proliferation of damaged cells. In fact, wtp53, a key regulator of cellular homeostasis, frequently referred to as the "guardian of the genome", fosters apoptosis and also inhibits VEGF-dependent angiogenesis, thereby opposing tumor growth and metastatization [61]. Concerning apoptosis, the selectivity of MM blend-mediated regulatory effect on this programmed cell death pathway was further confirmed analysing CASP9 and CASP3 expression patterns.

Specifically, the modulatory action of the MM blend on apoptotic pathway observed in cerebellar metastatic tissue was highlighted by the presence of enhanced CASP9 levels reported in MU-care treated mice only, thus evidencing increased cell death events in the metastases after supplementation. Our findings are in agreement with previous literature data revealing that a reduction in CASP9 expression levels can represent a tumour escape mechanism of apoptosis [62]. Furthermore, caspase-9 inhibition was related to increased resistance of cancer cells to chemotherapeutics treatment [63].

Then, following the known molecular apoptotic cascade, with the aim to explore the occurrence of a specific apoptotic pathway, we addressed the effect of MU-care supplement on CASP3. Caspase-3 is a key regulator of the apoptotic response, chiefly involved in tumorigenesis. Several studies demonstrated that increased CASP3 expression levels are closely associated with adverse breast cancer-specific patients' survival [64]. Notably, showing a different expression trend compared to other aforementioned markers, a lack of a direct CASP3 apoptotic effect on metastases was revealed.Concerning Hsp70, evidence that it is overexpressed in cancer, and that its high expression correlates with increased tumour grade and poor prognosis, is extensive also in patients affected by breast cancer [65]. In particular, this chaperon acts endowing malignant cells selective advantage by suppressing multiple apoptotic pathways (including autophagy), regulating necrosis, evading cellular senescence program, also promoting angiogenesis and thus supporting metastatization [66,67] Based on its clinical significance, assessment of several Hsp70-based immunotherapy protocols is still ongoing in clinical trials, together with the experimental use of Hsp70 inhibitors as promising chemotherapeutics. In accordance with these literature evidences, our current results in cerebellum revealed a strikingly high Hsp70-immunopositive cell density in metastases, with a value 50–100-fold higher compared to all other evaluated markers in the same metastatic regions. Notably, a significant reduction of Hsp70 levels (in terms of both cell density and OD) was assessed equally in metastases and parenchyma (namely, PCs) of MU-care treated mice compared to

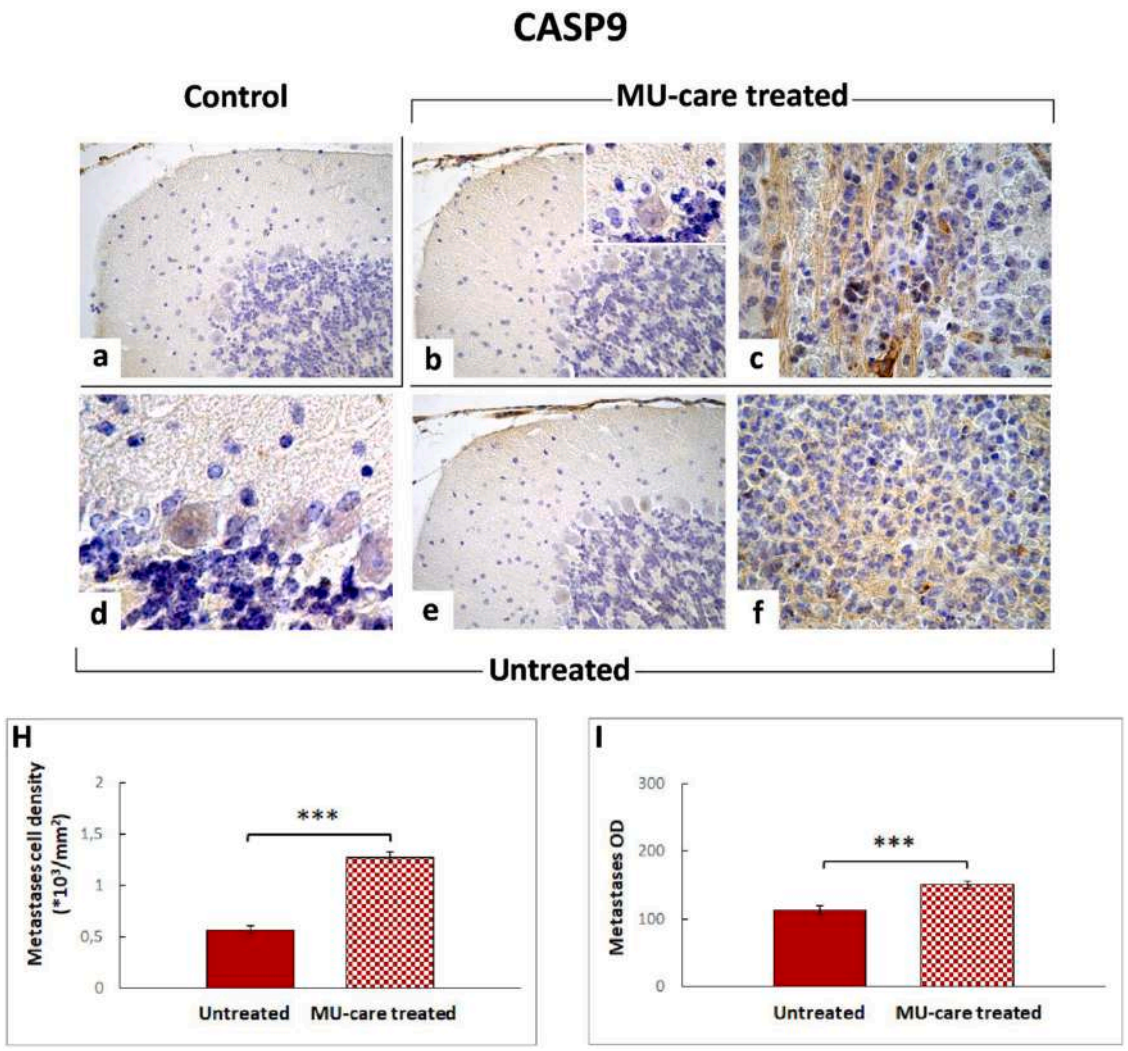

Fig. 8. Immunohistochemical labelling for CASP9 in healthy control (**a**), MU-care treated (***b, c***), and Untreated (**d–f**) mice. CASP9 immunopositivity was perceivable in the PCs soma of MU-care treated (**b**) and Untreated animals (**d, e**). An intensely marked immunolabeling was also evident in metastatic areas of MU-care treated mice (**c**). Immunopositivity was also noticeable in Untreated animals' metastases (**f**). Light microscopy magnification: 40 × (**a, b, e**); 60 × (**c, d, f,** insert in **b**). **Panels H** and **I**: Histograms illustrating quantitative evaluation of immunopositive metastases cell density and OD, respectively. *p* value calculated by unpaired Student's t-test: (***) < 0.001.

Table 5
Quantitative evaluation of initiator and effector caspases, i.e. CASP9 and CASP3, in cerebellar metastatic area.

	CASP9		CASP3	
	Cell density	*OD*	*Cell density*	*OD*
Untreated MU-care treated	0.57 ± 0.04 1.28 ± 0.05	113.40 ± 6.49 150.31 ± 5.98	0.49 ± 0.04 0.50 ± 0.04	187.35 ± 5.16 193.65 ± 5.39

Untreated animals. This extremely significant decrease was accompanied by the above-mentioned lessening in PCNA expression. This concurrent trend appeared in line with previous clinical findings reporting a conversely positive correlation between elevated PCNA and Hsp70 expression levels measured in human breast cancer patients [65].

The significant increase of CASP9 expression levels in metastatic areas of MU-care animals, was not succeeded by the expected increase of CASP3 in the same tissue, opening the hypothesis that other caspase effectors could be involved in the proapoptotic effects. Furthermore, the significant reduction of apoptosis-inducing factor (AIF) in metastases of syngeneic tumour-bearing mice suggests that metastatic BC cells would be able to escape cellular mechanisms which lead to both caspase-dependent and -independent apoptotic pathways, nonetheless leaving the hypothesis standing that an involvement of other cell death mechanisms would occurred in metastatic cells after MM supplementation.

Whether this beneficial action is to be ascribable to a direct β-glucans or other MM blend active metabolites effect, carried out crossing the BBB, or rather to a systemic anti-tumoral, immunomodulatory MM extract effect still needs to be clarified. We could even hypothesize that both mechanisms may contribute to the observed CNS outcomes. To elucidate this hypothesis, our recent in vitro data investigated the possible contribution of micotherapy in the fight against GBM and its synergic effect with a newly synthesized platinum-based compound, using human GBM U251 cells [68]. Interestingly, in line with the present in vivo results, we demonstrated that MU-care was able to regulate cell cycle, control cellular redox state, and to induce regulated form of necrosis, such as ferroptosis in U251 cells, thereby supporting the efficacy of this new combined therapy.

In conclusion, these data demonstrated that MU-care inhibit breast cancer cerebellar metastasis both by (i) a direct and specific inhibition of cerebellar metastatization pattern typical of TNBC, as well as by (ii) regulating apoptosis and proliferation-related genes. Therefore, this

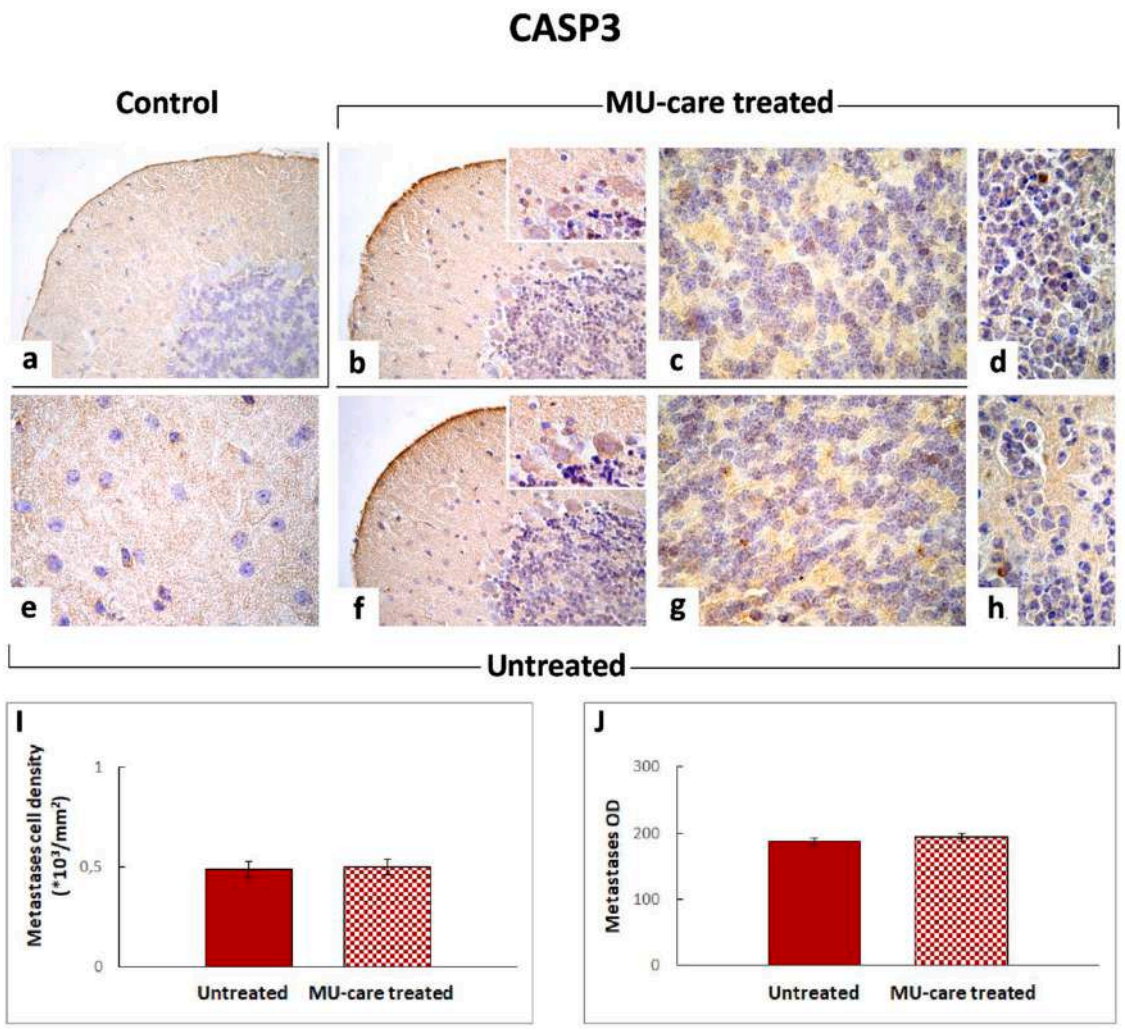

Fig. 9. Representative micrographs showing CASP3 immunohistochemical expression in healthy control (**a**), MU-care treated (**b-d**) and Untreated (**e–h**) mice. An intensely marked CASP3 immunopositivity was observed in ML of Untreated mice (**e, f**) as well as in IGL of both MU-care treated (**c**) and Untreated animals (**g**). Few immunolabeled cells were spotted in metastases, both in Untreated (**h**) and MU-care treated (**d**) mice. Light microscopy magnification: 40 × (**a, b, f**); 60 × (**c, d, e, g, h,** insert in **b** and **f**). **Panels I** and **J**: Histograms demonstrating quantitative data concerning metastases cell density and OD, respectively. *p* value calculated by unpaired Student's t-test: > 0.05.

MU-care-induced pleiotropic action make this MM blend a powerful, non-pharmacological therapeutic tool to be employed in integrative oncology, aiding the fight against TNBC-derived BM occurrence. Fig. 12.

4. Materials and methods

4.1. MU-care blend: raw materials from medicinal mushrooms, extraction procedure, beta-glucan title

The MU-care blend consisted of a mixture of five fungal species, produced and supplied by A.V.D. Reform s.r.l. (Noceto, Parma, Italy), and registered by the Italian Ministry of Health as a dietary supplement (registration number 627 I.5.i.h.2/2020/627). The detailed MU-care supplement (batch n. XMBLEND25032020) composition is reported here following (Table 7).

By sequencing Internal Transcribed Spacer (ITS) regions of nuclear DNA and confirming the ID code, specific MM species strains were established (for primers selection, see [29]). The PCR products were purified and sequenced by Eurofins Genomics (Konstanz, Germany). The identification was performed by using NCBI Nucleotide Blast software, version 2.9.0 (Table 7, ID code).

Subsequently, the sporophores and mycelia were cultivated for two to four months at 23 °C in a 1000 ± 100 ppm CO_2 atmosphere. After harvesting, the fresh material was extracted for 3 h at 95 °C in distilled water plus ethanol 10% (1 kg of raw material in 15 L of water/ethanol solution). After extraction, the fluid component was dehydrated until it reached less than 7% of humidity. Dry extracts were grounded and blended to obtain the 20% of each selected mushroom in the MU-care (Table 7).

All raw materials and final products were regularly verified following GMP, accordingly to the Hazard Analysis and Critical Control Points (HACCP) system, also to ensure traceability, even in accordance to Regulation (EC) No. 178/2002.

Finally, using a β-Glucan Assay Kit (Megazyme, LTD., Wicklow, Ireland), the MU-care blend was checked to measure the polysaccharide content, expressed as total (α plus β) glucan content and 1,3–1,6 β-glucans. This analysis revealed a polysaccharide content more than 30%. Out of this percentage (30%), > 15% were identified as 1,3–1,6 β-glucans, the main key active ingredients in MU-care.

4.2. Animals and experimental design

Wild-type (strain BALB/c) female (n = 34) mice (Charles River Italia, Calco, Italy) entered the Animal Care Facility of the University of Pavia

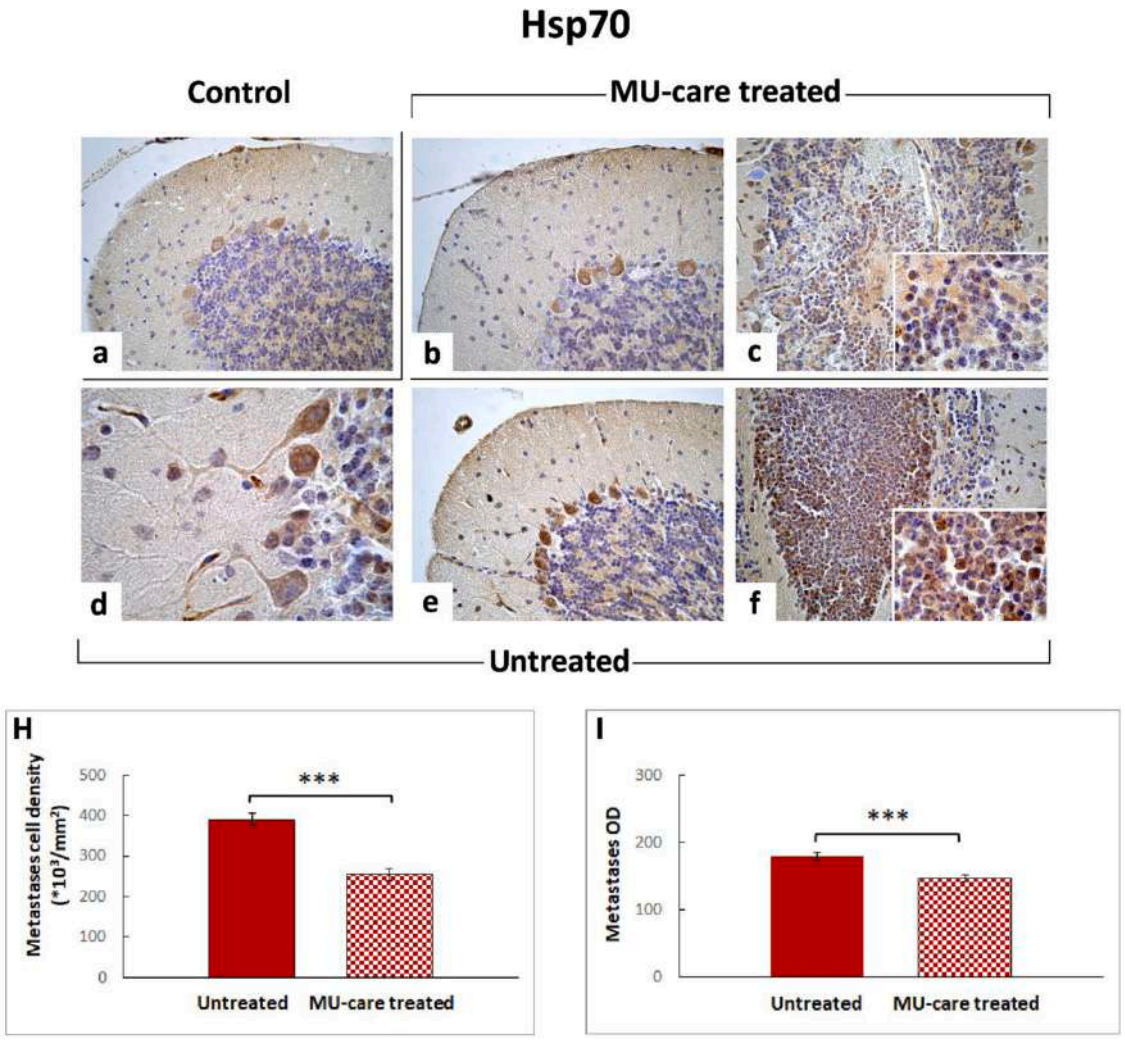

Fig. 10. Representative serial cerebellar sections immunostained for Hsp70 in healthy control (**a**), MU-care treated (**b, c**), and Untreated (**d–f**) mice. A marked Hsp70 immunopositivity was detectable in the PCs (soma and main dendrites) of healthy controls (**a**), MU-care treated (**b, c**) and Untreated (**d, e**) animals. An extremely intense immunolabeling was also evident in the metastases of Untreated mice (f). Immunopositivity was also strong in metastases of MU-care treated animals (**c**). Light microscopy magnification: 40 × (**a, b, c, e, f**); 60 × (**d,** insert in **c**, insert in **f**). **Panels H** and **I**: Quantification of immunopositive metastases cell density and OD, respectively. *p* value calculated by unpaired Student's t-test: (***) < 0.001.

Table 6
Quantitative measurement of essential markers of apoptosis and parthanatos, i.e. Hsp70 and AIF, respectively, in metastases.

	HSP70		**AIF**	
	Cell density	*OD*	*Cell density*	*OD*
Untreated	390.63 ± 15.32	179.92 ± 5.90	0.60 ± 0.05	124.67 ± 5.70
MU-care treated	254.16 ± 15.82	146.81 ± 4.26	0.66 ± 0.04	146.67 ± 4.43

at ~8 weeks of age. The pathogen-free mice were acclimatized for three weeks before experiments, housed in temperature and humidity-controlled (21 ± 2 °C with humidity at 50 ± 10%) vivaria (two animals/cage) under a 12:12 h light/dark cycle throughout the experiments. 12:12 h light: dark cycles. Mice had ad libitum access to food and water. Experimental procedures were performed in agreement with the European Council Directive 2010/63/EU on the care and use of laboratory animals, also following the guidelines established by the institution's animal welfare committee, the Ethics Committee of Pavia University (Ministry of Health, License number 364/2018-PR, approval date:17 May 2018). All animals employed have been treated humanely, with due concern for distress and discomfort alleviation.

To prevent any bias in study results, researchers were blinded to the group assignment for all experimental procedures.

For a three month-period, after acclimatization and until sacrifice, 16 (MU-care treated) out of 34 mice were provided with a Micotherapy U-care drink, consisting of a mixture of mycelium plus sporophores extracts of five MM species, including (20%) *Agaricus blazei* Murrill, *Agaricaceae*, (20%) *Ganoderma lucidum* (Curtis) P. Karst., *Polyporaceae*, (20%) *Grifola frondosa* (Dicks.) Gray, *Grifolaceae*, (20%) *Lentinula edodes* (Berk.) Pegler, *Omphalotaceae*, and (20%) *Ophiocordyceps sinensis* (Berk.) G.H. Sung, J.M. Sung, Hywel-Jones & Spatafora, *Ophiocordycipitaceae*. The fungal scientific names are currently accepted according to Index fungorum (http://www.indexfungorum.org/). The blend was solubilized in water and the dose of 4 mg supplement/day/mouse (corresponding to 0.16 g/kg/day) was selected to simulate human oral supplementation. The residual n = 14 not-treated mice (namely Untreated) and n = 4 healthy controls were fed without any supplementation. The syngeneic tumour-bearing mice were generated by injecting 4T1 cells (10^6) into the nape of the neck of the BALB/c female animals. The healthy controls were inoculated with the vehicle (i.e. phosphate-buffer saline, PBS). The quality of life (QoL), measured in terms of body weight gain and water consumption, and locomotor activity were

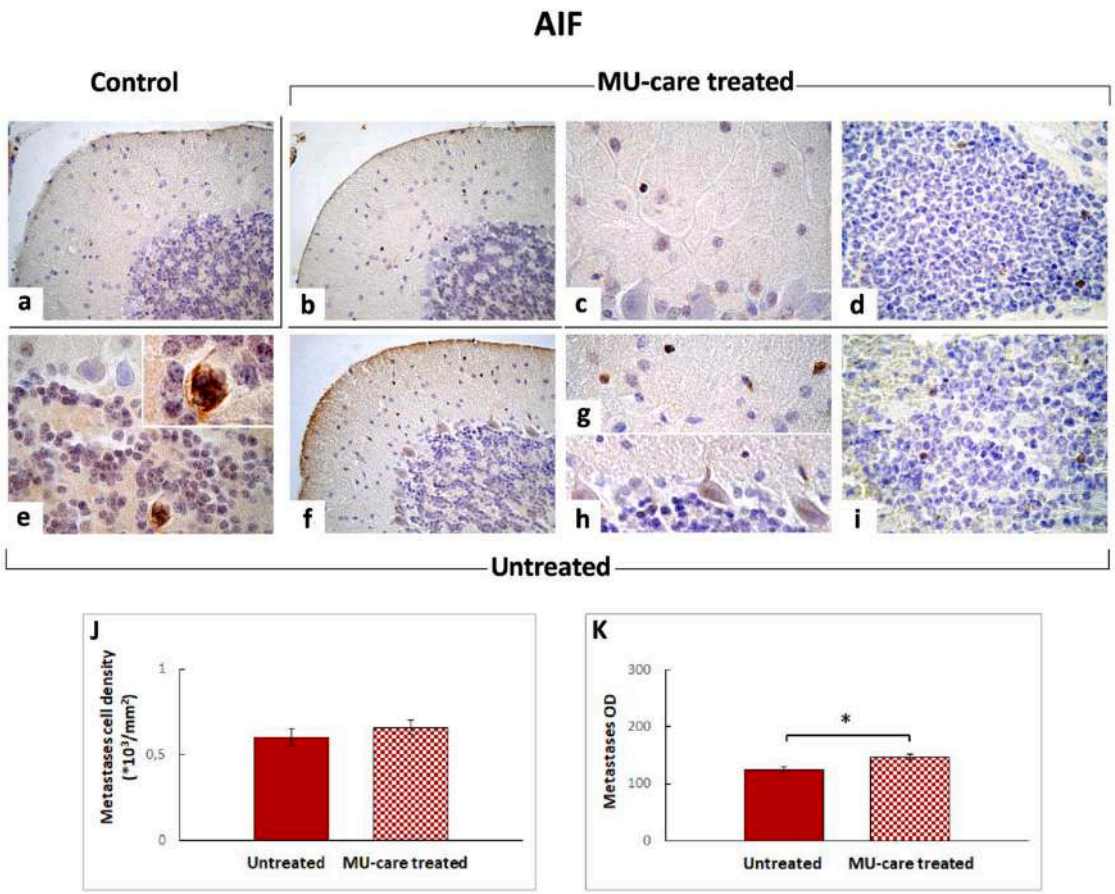

Fig. 11. Representative cerebellar sections immunostained for AIF in healthy control (**a**), MU-care treated (**b-d**), and Untreated (**e-i**) mice. An intensely marked AIF immunopositivity was observed in IGL of Untreated mice (**e**) as well as in ML of both MU-care treated (**c**) and Untreated (**g**) animals. Several immunolabeled cells were spotted in metastases, both in Untreated (**i**) and MU-care treated (**d**) mice. Light microscopy magnification: 40 × (**a, b, f**); 60 × (**c, d, e, g, h, i**); 100x (insert in **e**). **Panels J** and **K**: Histograms demonstrating quantitative data concerning metastases cell density and OD, respectively. *p* value calculated by unpaired Student's t-test: (*) < 0.05.

checked every day. Experimental time plan comprised: T0, animals' randomization; T1, Micotherapy U-care oral supplementation initiation (for MU-care treated mice, only); T2 (about 2 months later), 4T1 cells inoculation in both Untreated and MU-care treated mice; T3 (about 20 days later): monitoring and evaluations beginning; T4 (about 15 days later): monitoring and evaluations ongoing. At T1 and T3, the locomotor activity was examined by using a behavioural test. Twenty-four hours after T4, mice were euthanized and cerebella were removed and processed for histopathological and immunohistochemical investigations.

4.3. Emergence test

At chosen timepoints, i.e. T1 and T3, all mice performed the emergence task, a spontaneous behavioural test being a variant of the open-field test, properly designed to reduce anxiety by providing a safe enclosure within the open field. The emergence task was used to assess exploratory behaviour and locomotor activities. The free exploration test consisted of housing mice in a compartment prior to giving the animal a free choice between a familiar compartment and a novel one. During the test, each animal was located in a familiar environment (cage measures: 13 cm x 15 cm x 33 cm, length x width x height) with a hole in one side (4 cm wide and 5 cm long) through which it could emerge in a larger arena (60 cm x 90 cm, width x length) without walls but with a laminated floor. The observation lasted 8 min/mouse, during the free exploring of the arena. Three locomotor parameters were assessed: total distance (cm), mean speed (cm/s), and resting time (s). The animals' movement was tracked and quantified using a SMART video automated tracking system (2 Biological Instruments, Besozzo, Varese, Italy) with 40 ms/point sampling time and a Sony CCD colour video camera (PAL; Sony Europe B.V.- Italian headquarters, Milan, Italy) [69]. Emergence test results were expressed as a score index, calculated as reported below.

4.4. Histology and immunohistochemistry

4.4.1. Cerebellar tissue

Thirty-five days after 4T1 injection, mice were deeply anesthetized before decapitation by using isoflurane inhalation (Aldrich, Milwaukee, WI, USA). Cerebella were immediately excised as previously described [57], washed in 0.9% NaCl, and post-fixed by immersion for 7 h in 4% paraformaldehyde in 0.1 M phosphate buffer (pH 7.4), dehydrated through a graded series of ethanol and finally embedded in Paraplast X-TRA. Using a manual rotatory microtome, sagittal Section (8 μm thick) of cerebellar vermis, were cut serially and collected on silane-coated slides.

4.4.2. Morphological and histochemical evaluations

To reveal cerebellar cortex cytoarchitecture and estimate potential structural alterations by light microscopy, Haematoxylin and Eosin (H&E), Nissl and Picrosirius Red (PSR) staining were executed as previously described [70–73]. Briefly, serial tissue sections were processed as follows: (i) *H&E*: 10 min staining with Carazzi's Haematoxylin (Bio-Optica Milano S.p.A., Milano, Italy), followed by 20 min wash in running tap water and counterstaining with 1% eosin solution

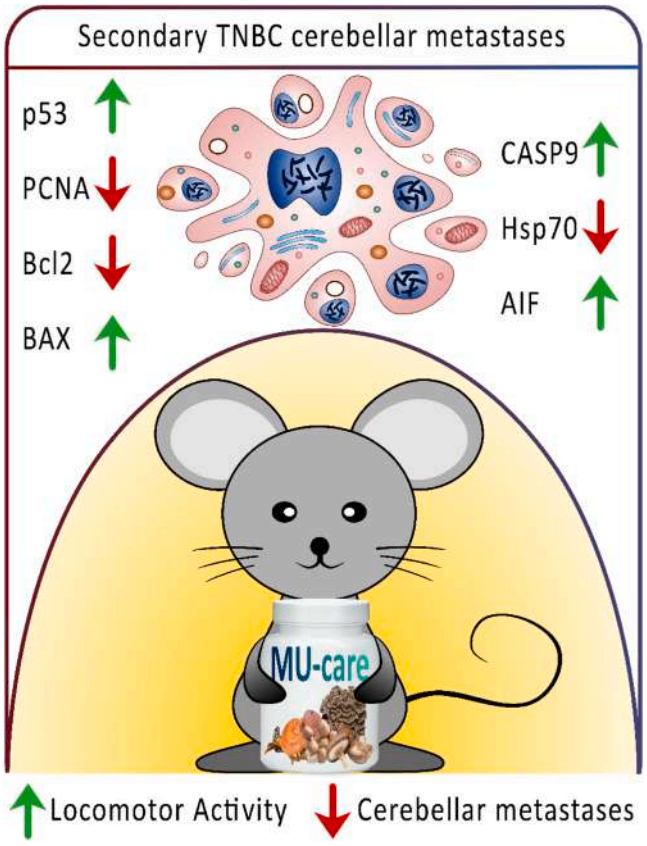

Fig. 12. Illustrative picture summarizing main findings and take-home message.

Table 7
MU-care blend: MM composition.

Medicinal mushroom	Fungal part	%	ID code
Agaricus blazei	Fruiting body	20	7700
Ganoderma lucidum	Fruiting body	20	Gac
Grifola frondosa	Fruiting body	20	Gf3
Lentinula edodes	Fruiting body	20	Le.ed.1
Ophiocordyceps sinensis	Fruiting body + mycelium	20	Cm2

(Bio-Optica Milano S.p.A., Milano, Italy); the nucleic acids stain violet to dark blue while the proteins stain pink to red; (ii) *Nissl*: 1% cresyl violet (Sigma, St. Louis, MO, USA) solution for 3 min followed by differentiation in acetic acid in 100% ethanol (at 1:50,000 dilution) for 5 s; (iii) *PSR*: 1 h staining with Picrosirius Red solution (0.1% of Sirius Red in saturated aqueous picric acid), followed by a wash in 5% acidified water [71–73]. Lastly, all differently stained cerebellar sections were dehydrated in ethanol, cleared in xylene, and mounted in Eukitt (Kindler, Freiburg, Germany).

4.4.3. Immunohistochemistry

With the aim at preventing potential staining discrepancies due to minor changes in the protocol, immunocytochemical reactions were performed simultaneously on slides from different experimental groups. Immunohistochemistry was carried out using commercial antibodies on murine cerebellar specimens, to localize presence and distribution of different cell death markers: (i) Proliferating Cell Nuclear Antigen (PCNA), (ii) B-cell lymphoma 2 (Bcl-2), (iii) Bcl2 Associated X (BAX), (iv) Caspase 9 (CASP9), (v) Caspase 3 (CASP3), and (vi) 70 kDa Heat shock protein (Hsp70).

After being de-paraffinized in xylene and rehydrated, cerebellar sections of healthy controls, Untreated, and MU-care treated mice underwent antigen retrieval and were then incubated overnight at room temperature in a dark moist chamber with selected monoclonal and polyclonal primary antibodies (Table 8) diluted in PBS.

Subsequently, proper biotinylated secondary antibodies (Table 8) and an avidin biotinylated horseradish peroxidase complex (Vector Laboratories, Burlingame, CA, USA) were employed to uncover the antigen/antibody interaction sites. The 3,3'-diaminobenzidine tetrahydrochloride peroxidase substrate (Sigma, St. Louis, MO, USA) was utilized as the chromogen, while the nuclear counterstaining was done using Carazzi's Haematoxylin.

Next, sections were dehydrated in ethanol, cleared in xylene, and mounted in Eukitt (Kindler, Freiburg, Germany). As negative untreated, some tissues were incubated with PBS in absence of primary antibodies: no immunoreactivity was detected in this condition.

4.4.4. Microscopes, imaging systems and histochemical/immunohistochemical measurements

After morphological and histochemical reactions, slides were observed and scored using a bright-field Zeiss Axioscop Plus 612 microscope (Carl Zeiss S.p.A., Milan, Italy). Five slides (about 18–20 randomized sections) per animal were analysed; 5 microscopic fields were examined in each section for each mouse per time/condition. The images were recorded with an Olympus Camedia C-5050 digital camera and stored on a PC running Olympus software (Olympus Italia, Segrate, MI, Italy). Following immunohistochemical procedures, slides were examined using an Olympus BX51 optical microscope (model BX51TF). The images were acquired with an Olympus CAMEDIA C4040ZOOM camera (Olympus Italia, Segrate, MI, Italy). For each marker, six slides (about 30 sections) per animal were analysed. Cerebellar specimens from all experimental group displayed different immunolabelling extent and the figures show the most representative changes for each immunohistochemical reaction. The diverse labelling extents were evaluated on acquired digitized section images under exposure time avoiding any pixel saturation effect. The labelling intensity was measured exploiting densitometric analysis (Image-J 1.46p; NIH, Bethesda, MA, USA). The mask shape was adjusted depending on the spatial distribution of the cell type and/or tissue specimens under measurement; the labelling was measured as the mean intensity value over the area. The immunocytochemical intensity, specified as optical density (OD), was assessed in 3 randomized images/section (making at least 10 measurements/image) per 5 slides/animal from each experimental group, with the operator blinded to the experimental condition. Results were recorded on Microsoft Office Excel Software spreadsheets and the analysis was achieved using the ImageJ software. The following additional measurements were carried out: immunopositive metastases and micrometastases density count (number of metastases and micrometastases/area in cm^2); immunopositive cells density count ($*10^3$) (number of immunopositive cells/area in mm^2).

4.5. Statistics

Data were expressed as means ± standard error of the mean (SEM). The Bartlett and Shapiro Wilk Tests was used to establish and confirm the normality of parameters. Then, data were analysed to verify statistically significant differences. One-way ANOVA and Bonferroni post-hoc tests were performed to compare the different groups as regards to the behavioural test analysis. The statistical analysis for histology (namely H&E) was performed using unpaired Student's t-test. Concerning Picrosirius Red staining, one-way ANOVA followed by Bonferroni's post-hoc test was carried out. Regarding immunohistochemistry, unpaired Student's t-test was employed for metastatic areas to measure significant changes between MU-care treated and Untreated mice. The differences were considered statistically significant for $p < 0.05$ (*), $p < 0.01$ (**), and $p < 0.001$ (***). Statistical analyses were performed by using GraphPad Prism 7.0 (GraphPad Software Inc., La Jolla, CA, USA) and R software.

Table 8
Primary/secondary antibodies employed for light microscopy experimental procedures.

	Antigen	Immunogen	Manufacturer, Species, Mono-Polyclonal, Cat./Lot. No., RRID	Dilution
Primary antibodies	Anti-B-Cell Leukemia/ Lymphoma 2 protein (N-19)	Purified antibody raised against a peptide mapping at the N-terminus of Bcl-2 of human origin	Santa Cruz Biotechnology (Santa Cruz, CA, USA), Rabbit polyclonal IgG, Cat# sc-492, RRID: AB_2064290	1:100
	Anti-Bcl-2-associated X protein (P-19)	Purified antibody raised against a peptide mapping at the amino terminus of BAX of mouse origin	Santa Cruz Biotechnology (Santa Cruz, CA, USA), Rabbit polyclonal IgG, Cat# sc-526, RRID: AB_2064668	1:100
	Anti- caspase-3 (31A1067)	Purified antibody raised against an epitope mapping between amino acids 50–86 of caspase-3 p17 of human origin	Santa Cruz Biotechnology (Santa Cruz, CA, USA), Mouse monoclonal IgG, Cat# sc-56053, RRID: AB_781826	1:100
	Anti-Caspase 9 p35 (A-9)	Purified antibody raised against amino acids 100–270 of caspase-9 p35 of human origin.	Santa Cruz Biotechnology (Santa Cruz, CA, USA), Mouse monoclonal IgG, Cat# sc-133109, RRID: AB_2073466	1:100
	Anti-HSP 70/HSC 70 (5A5)	Purified antibody raised against recombinant HSP 70/HSC 70 of human origin	Santa Cruz Biotechnology (Santa Cruz, CA, USA), Mouse monoclonal IgG, Cat# sc-32239, RRID: AB_627759	1:100
	Anti-apoptosis-inducing factor (E-1)	Purified antibody raised against amino acids 1–300 of AIF of human origin	Santa Cruz Biotechnology (Santa Cruz, CA, USA), Mouse monoclonal IgG, Cat# sc-13116, RRID: AB_626654	1:100
	Anti-p53 (Ab-5)	Purified antibody raised against the ~53 kDa wild type p53 protein of mouse origin	Sigma-Aldrich (St. Louis, MO, USA), Mouse monoclonal IgG2a, Cat# OP33–100UG, RRID: AB_564977	1:100
	Anti-Proliferating Cell Nuclear Antigen (Ab-1)	Purified antibody raised against the ~37 kDa PCNA protein of mouse origin	Sigma-Aldrich (St. Louis, MO, USA), Mouse monoclonal IgG2a, Cat# NA03–200UG, RRID: AB_213111	1:500
Secondary antibodies	Biotinylated goat anti-rabbit IgG	Gamma immunoglobulin	Vector Laboratories (Burlingame, CA, USA), Goat, lot# PK-6101, RRID: AB_2336820	1:200
	Biotinylated horse anti-mouse IgG	Gamma immunoglobulin	Vector Laboratories (Burlingame, CA, USA), Horse, Cat# PK-6102, RRID: AB_2336821	1:200

5. Conclusions

Overall, our current findings revealed that MU-care display a selective anti-cancer effect addressed on cerebellar metastases, accompanied by a beneficial action on locomotor performances, thus supporting the efficacy of the MM blend on CNS secondary breast cancer. This MU-care played mechanism, inhibiting the metastatization pattern, triggering an imbalance between proliferation and cell death, hence driving to a significant apoptosis increase, could therefore representing a promising approach for patients' management as adjuvant therapy in the prevention and treatment of secondary breast cancer in brain. In fact, being the TNBC the most aggressive malignant BC, characterized by unresponsiveness to current clinical treatments, high relapse rate and typical metastatization pattern targeting CNS, the synergistic effect of MU-care supplement joint with conventional therapies targeting crucial cancer signalling pathways, i.e., proliferation and apoptosis, may hamper cellular and molecular processes feeding TNBC growth, thus delaying or even impeding the TNBC metastatic pattern, often associated with poor prognosis. Therefore, taken as a whole, the reported data support the use of MU-care oral supplementation as a new promising adjuvant strategy, in the field of integrative oncology, which could help to fight the occurrence of TNBC-derived BM.

Funding

This research was supported by the University of Pavia: Fondi Ricerca Giovani (FRG 2018). This research was also supported by Italian Ministry of Education, University and Research (MIUR): Dipartimenti di Eccellenza Program (2018–2022) Dept. of Biology and Biotechnology "L. Spallanzani", University of Pavia.

CRediT authorship contribution statement

Paola Rossi: Conceptualization, Methodology, Formal analysis, Writing – original draft, Writing – review & editing, Supervision, Project administration. **Elisa Roda**: Conceptualization, Methodology, Investigation, Formal analysis, Writing – original draft, Writing – review & editing, Supervision. **Fabrizio De Luca**: Methodology, Investigation, Formal analysis, Writing – original draft. **Daniela Ratto**: Software, Investigation, Formal analysis. **Anthea Desiderio**: Software, Validation. **Maria Teresa Venuti**: Software, Data curation. **Martino Ramieri**: Software, Validation. **Maria Grazia Bottone**: Resources. **Elena Savino**: Resources.

Conflict of interest statement

The authors declare that the research was conducted in the absence of any commercial or financial relationships that could be construed as a potential conflict of interest.

Acknowledgments

We thank Dr Carmine Di Iorio (Heallo S.r.l) for his technical assistance.

Author Contributions

E.R., P.R. conceived and designed the experiments. F.D.L., E.R., D.R., and P.R. performed the experiments and analysed the data. M.G.B. and E.S. contributed reagents, materials and analysis tools. A.D., M.T.V. and M.R. searched and reviewed the literatures. F.D.L., E.R. and P.R. drafted the paper. E.R. and P.R. critically revised the article. All authors provided critical feedback, helping shape the research and analysis. All

authors read and agreed to the published version of the manuscript.

References

[1] H. Sung, J. Ferlay, R.L. Siegel, M. Laversanne, I. Soerjomataram, A. Jemal, F. Bray, Global cancer statistics 2020: GLOBOCAN estimates of incidence and mortality worldwide for 36 cancers in 185 countries, CA Cancer J. Clin. 71 (2021) 209–249, https://doi.org/10.3322/caac.21660.

[2] I. Cetin, M. Topcul, Triple negative breast cancer, Asian Pac. J. Cancer Prev. 15 (2014) 2427–2431, https://doi.org/10.7314/APJCP.2014.15.6.2427.

[3] V. Ossovskaya, Y. Wang, A. Budoff, Q. Xu, A. Lituev, O. Potapova, G. Vansant, J. Monforte, N. Daraselia, Exploring molecular pathways of triple-negative breast cancer, Genes Cancer 2 (2011) 870–879, https://doi.org/10.1177/1947601911432496.

[4] P. Boyle, Triple-negative breast cancer: epidemiological considerations and recommendations, Ann. Oncol. 23 (6) (2012) vi7–vi12, https://doi.org/10.1093/annonc/mds187.

[5] F. Podo, L.M.C. Buydens, H. Degani, R. Hilhorst, E. Klipp, I.S. Gribbestad, S. V. Huffel, H.W.M. van Laarhoven, J. Luts, D. Monleon, et al., Triple-negative breast cancer: present challenges and new perspectives, Mol. Oncol. 4 (2010) 209–229, https://doi.org/10.1016/j.molonc.2010.04.006.

[6] D.C. Brady-West, D.A. McGrowder, Triple negative breast cancer: therapeutic and prognostic implications, Asian Pac. J. Cancer Prev. 12 (2011) 2139–2143.

[7] E. Roda, F. De Luca, C. Di Iorio, D. Ratto, S. Siciliani, B. Ferrari, F. Cobelli, G. Borsci, E.C. Priori, S. Chinosi, et al., Novel medicinal mushroom blend as a promising supplement in integrative oncology: a multi-tiered study using 4t1 triple-negative mouse breast cancer model, Int. J. Mol. Sci. 21 (2020) 3479, https://doi.org/10.3390/ijms21103479.

[8] C. Neophytou, P. Boutsikos, P. Papageorgis, Molecular mechanisms and emerging therapeutic targets of triple-negative breast cancer metastasis, Front. Oncol. 8 (2018) 31, https://doi.org/10.3389/fonc.2018.00031.

[9] K. Altundag, M.L. Bondy, N.Q. Mirza, S.-W. Kau, K. Broglio, G.N. Hortobagyi, E. Rivera, Clinicopathologic characteristics and prognostic factors in 420 metastatic breast cancer patients with central nervous system metastasis, Cancer 110 (2007) 2640–2647, https://doi.org/10.1002/cncr.23088.

[10] U.Y. Arslan, Breast cancer subtypes and outcomes of central nervous system metastases, Breast (2011) 6.

[11] R.-H. Yeh, J.-C. Yu, C.-H. Chu, C.-L. Ho, H.-W. Kao, G.-S. Liao, H.-W. Chen, W.-Y. Kao, C.-P. Yu, T.-Y. Chao, et al., Distinct MR imaging features of triple-negative breast cancer with brain metastasis, J. Neuroimaging 25 (2015) 474–481, https://doi.org/10.1111/jon.12149.

[12] N. Niikura, J. Liu, N. Hayashi, E.A. Mittendorf, Y. Gong, S.L. Palla, Y. Tokuda, A. M. Gonzalez-Angulo, G.N. Hortobagyi, N.T. Ueno, Loss of human epidermal growth factor receptor 2 (HER2) expression in metastatic sites of HER2-overexpressing primary breast tumors, J. Clin. Oncol. 30 (2012) 593–599, https://doi.org/10.1200/JCO.2010.33.8889.

[13] S.Y. Jung, M. Rosenzweig, S.M. Sereika, F. Linkov, A. Brufsky, J.L. Weissfeld, Factors associated with mortality after breast cancer metastasis, Cancer Causes Control 23 (2012) 103–112, https://doi.org/10.1007/s10552-011-9859-8.

[14] S. Pakneshan, D. Safarpour, F. Tavassoli, B. Jabbari, Brain metastasis from ovarian cancer: a systematic review, J. Neurooncol. 119 (2014) 1–6, https://doi.org/10.1007/s11060-014-1447-9.

[15] A.H. Graf, W. Buchberger, H. Langmayr, K.W. Schmid, Site preference of metastatic tumours of the brain, Virchows Arch. A Pathol. Anat. Histopathol. 412 (1988) 493–498, https://doi.org/10.1007/BF00750584.

[16] C. Bailleux, L. Eberst, T. Bachelot, Treatment strategies for breast cancer brain metastases, Br. J. Cancer 124 (2021) 142–155, https://doi.org/10.1038/s41416-020-01175-y.

[17] R. Rostami, S. Mittal, P. Rostami, F. Tavassoli, B. Jabbari, Brain metastasis in breast cancer: a comprehensive literature review, J. Neurooncol. 127 (2016) 407–414, https://doi.org/10.1007/s11060-016-2075-3.

[18] P.D. Bos, X.H.-F. Zhang, C. Nadal, W. Shu, R.R. Gomis, D.X. Nguyen, A.J. Minn, M. J. van de Vijver, W.L. Gerald, J.A. Foekens, et al., Genes that mediate breast cancer metastasis to the brain, Nature 459 (2009) 1005–1009, https://doi.org/10.1038/nature08021.

[19] D.P. Fitzgerald, D. Palmieri, E. Hua, E. Hargrave, J.M. Herring, Y. Qian, E. Vega-Valle, R.J. Weil, A.M. Stark, A.O. Vortmeyer, et al., Reactive glia are recruited by highly proliferative brain metastases of breast cancer and promote tumor cell colonization, Clin. Exp. Metastasis 25 (2008) 799–810, https://doi.org/10.1007/s10585-008-9193-z.

[20] S.P. Wasser, Medicinal mushrooms in human clinical studies. Part I. Anticancer, oncoimmunological, and immunomodulatory activities: a review, Int. J. Med. Mushrooms 19 (2017) 279–317, https://doi.org/10.1615/IntJMedMushrooms.v19.i4.10.

[21] P. Rossi, R. Difrancia, V. Quagliariello, E. Savino, P. Tralongo, C.L. Randazzo, M. Berretta, B-glucans from grifola frondosa and ganoderma lucidum in breast cancer: an example of complementary and integrative medicine, Oncotarget 9 (2018) 24837–24856, https://doi.org/10.18632/oncotarget.24984.

[22] K. Tanaka, Y. Matsui, S. Ishikawa, T. Kawanishi, M. Harada, Oral ingestion of lentinula edodes mycelia extract can restore the antitumor T cell response of mice inoculated with colon-26 cells into the subserosal space of the cecum, Oncol. Rep. 27 (2012) 325–332, https://doi.org/10.3892/or.2011.1549.

[23] J. Jiang, D. Sliva, Novel medicinal mushroom blend suppresses growth and invasiveness of human breast cancer cells, Int. J. Oncol. 37 (2010) 1529–1536, https://doi.org/10.3892/ijo_00000806.

[24] B.G.J. Moerings, P. de Graaff, M. Furber, R.F. Witkamp, R. Debets, J.J. Mes, J. van Bergenhenegouwen, C. Govers, Continuous exposure to non-soluble β-glucans induces trained immunity in M-CSF-differentiated macrophages, Front. Immunol. 12 (2021), 672796, https://doi.org/10.3389/fimmu.2021.672796.

[25] L. Steimbach, A.V. Borgmann, G.G. Gomar, L.V. Hoffmann, R. Rutckeviski, D.P. de Andrade, F.R. Smiderle, Fungal beta-glucans as adjuvants for treating cancer patients - a systematic review of clinical trials, Clin. Nutr. 40 (2021) 3104–3113, https://doi.org/10.1016/j.clnu.2020.11.029.

[26] N. Kodama, K. Komuta, H. Nanba, Effect of maitake (Grifola Frondosa) D-fraction on the activation of NK cells in cancer patients, J. Med. Food 6 (2003) 371–377, https://doi.org/10.1089/109662003772519949.

[27] G. Deng, H. Lin, A. Seidman, M. Fornier, G. D'Andrea, K. Wesa, S. Yeung, S. Cunningham-Rundles, A.J. Vickers, B. Cassileth, A phase I/II trial of a polysaccharide extract from grifola frondosa (maitake mushroom) in breast cancer patients: immunological effects, J. Cancer Res. Clin. Oncol. 135 (2009) 1215–1221, https://doi.org/10.1007/s00432-009-0562-z.

[28] P. Singh, B. Lim, Targeting apoptosis in cancer, Curr. Oncol. Rep. 24 (2022) 273–284, https://doi.org/10.1007/s11912-022-01199-y.

[29] E. Roda, F. De Luca, C.A. Locatelli, D. Ratto, C. Di Iorio, E. Savino, M.G. Bottone, P. Rossi, From a medicinal mushroom blend a direct anticancer effect on triple-negative breast cancer: a preclinical study on lung metastases, Molecules (2020) *25*, https://doi.org/10.3390/molecules25225400.

[30] M. Berretta, A. Morra, R. Taibi, F. Monari, N. Maurea, M. Ippolito, U. Tirelli, F. Fiorica, L. Montella, G. Facchini, et al., Improved survival and quality of life through an integrative, multidisciplinary oncological approach: pathophysiological analysis of four clinical cancer cases and review of the literature, Front. Pharmacol. 13 (2022), 867907, https://doi.org/10.3389/fphar.2022.867907.

[31] E. D'Angelo, P. Rossi, G. De Filippi, J. Magistretti, V. Taglietti, The relationship between synaptogenesis and expression of voltage-dependent currents in cerebellar granule cells in situ, J. Physiol. Paris 88 (1994) 197–207, https://doi.org/10.1016/0928-4257(94)90006-x.

[32] P. rossi, E. D'Angelo, V. Taglietti, Differential long-lasting potentiation of the NMDA and Non-NMDA synaptic currents induced by metabotropic and NMDA receptor coactivation in cerebellar granule cells, Eur. J. Neurosci. 8 (1996) 1182–1189, https://doi.org/10.1111/j.1460-9568.1996.tb01286.x.

[33] Y. Xiong, Y. Zhang, S. Xiong, A.E. Williams-Villalobo, A glance of P53 functions in brain development, neural stem cells, and brain cancer, Biology 9 (2020) 285, https://doi.org/10.3390/biology9090285.

[34] Y. Zhou, L. Liu, S. Tao, Y. Yao, Y. Wang, Q. Wei, A. Shao, Y. Deng, Parthanatos and its associated components: promising therapeutic targets for cancer, Pharmacol. Res. 163 (2021), 105299, https://doi.org/10.1016/j.phrs.2020.105299.

[35] M. Jeitler, A. Michalsen, D. Frings, M. Hübner, M. Fischer, D.A. Koppold-Liebscher, V. Murthy, C.S. Kessler, Significance of medicinal mushrooms in integrative oncology: a narrative review, Front. Pharmacol. 11 (2020) 1758, https://doi.org/10.3389/fphar.2020.580656.

[36] P. Nowakowski, R. Markiewicz-Żukowska, K. Gromkowska-Kępka, S.K. Naliwajko, J. Moskwa, J. Bielecka, M. Grabia, M. Borawska, K. Socha, Mushrooms as potential therapeutic agents in the treatment of cancer: evaluation of anti-glioma effects of coprinus comatus, cantharellus cibarius, lycoperdon perlatum and lactarius deliciosus extracts, Biomed. Pharmacother. 133 (2021), 111090, https://doi.org/10.1016/j.biopha.2020.111090.

[37] S.K. Panda, G. Sahoo, S.S. Swain, W. Luyten, Anticancer activities of mushrooms: a neglected source for drug discovery, Pharmaceuticals 15 (2022) 176, https://doi.org/10.3390/ph15020176.

[38] A. Sathyanesan, V. Gallo, Cerebellar contribution to locomotor behavior: a neurodevelopmental perspective, Neurobiol. Learn. Mem. 165 (2019), 106861, https://doi.org/10.1016/j.nlm.2018.04.016.

[39] S.M. Morton, A.J. Bastian, Cerebellar control of balance and locomotion, Neuroscientist 10 (2004) 247–259, https://doi.org/10.1177/1073858404263517.

[40] J.-B. Passot, D. Sheynikhovich, É. Duvelle, A. Arleo, Contribution of cerebellar sensorimotor adaptation to hippocampal spatial memory, PLoS One 7 (2012), e32560, https://doi.org/10.1371/journal.pone.0032560.

[41] J.N. Crawley, J.K. Belknap, A. Collins, J.C. Crabbe, W. Frankel, N. Henderson, R. J. Hitzemann, S.C. Maxson, L.L. Miner, A.J. Silva, et al., Behavioral phenotypes of inbred mouse strains: implications and recommendations for molecular studies, Psychopharmacology 132 (1997) 107–124, https://doi.org/10.1007/s002130050327.

[42] R.M. Saré, A. Lemons, C.B. Smith, Behavior testing in rodents: highlighting potential confounds affecting variability and reproducibility, Brain Sci. 11 (2021) 522, https://doi.org/10.3390/brainsci11040522.

[43] M. Chang, J.S. Saczynski, J. Snaedal, S. Bjornsson, B. Einarsson, M. Garcia, T. Aspelund, K. Siggeirsdottir, V. Gudnason, L.J. Launer, et al., Midlife physical activity preserves lower extremity function in older adults: age gene/environment susceptibility-reykjavik study, J. Am. Geriatr. Soc. 61 (2013) 237–242, https://doi.org/10.1111/jgs.12077.

[44] A. Middleton, S.L. Fritz, M. Lusardi, Walking speed: the functional vital sign, J. Aging Phys. Act. 23 (2015) 314–322, https://doi.org/10.1123/japa.2013-0236.

[45] H. Mehmet, S.R. Robinson, A.W.H. Yang, Assessment of gait speed in older adults, J. Geriatr. Phys. Ther. 43 (2020) 42–52, https://doi.org/10.1519/JPT.0000000000000224.

[46] P. Mahlknecht, S. Kiechl, J. Willeit, W. Poewe, K. Seppi, Motoric cognitive risk syndrome: multicenter incidence study, Neurology 85 (2015) 388–389, https://doi.org/10.1212/01.wnl.0000470376.04336.ea.

[47] E. Buckley, C. Mazzà, A. McNeill, A systematic review of the gait characteristics associated with cerebellar ataxia, Gait Posture 60 (2018) 154–163, https://doi.org/10.1016/j.gaitpost.2017.11.024.

[48] A. Droby, M.M. El Mendili, N. Giladi, J.M. Hausdorff, I. Maidan, A. Mirelman, Gait and cognitive abnormalities are associated with regional cerebellar atrophy in elderly fallers - a pilot study, Gait Posture 90 (2021) 99–105, https://doi.org/10.1016/j.gaitpost.2021.08.012.
[49] Q. Tian, S.A. Studenski, M. Montero-Odasso, C. Davatzikos, S.M. Resnick, L. Ferrucci, Cognitive and neuroimaging profiles of older adults with dual decline in memory and gait speed, Neurobiol. Aging 97 (2021) 49–55, https://doi.org/10.1016/j.neurobiolaging.2020.10.002.
[50] L.F. Koziol, D. Budding, N. Andreasen, S. D'Arrigo, S. Bulgheroni, H. Imamizu, M. Ito, M. Manto, C. Marvel, K. Parker, et al., Consensus paper: the cerebellum's role in movement and cognition, Cerebellum 13 (2014) 151–177, https://doi.org/10.1007/s12311-013-0511-x.
[51] C.J. Stoodley, J.D. Schmahmann, Functional topography in the human cerebellum: a meta-analysis of neuroimaging studies, Neuroimage 44 (2009) 489–501, https://doi.org/10.1016/j.neuroimage.2008.08.039.
[52] K. Kansal, Z. Yang, A.M. Fishman, H.I. Sair, S.H. Ying, B.M. Jedynak, J.L. Prince, C. U. Onyike, Structural cerebellar correlates of cognitive and motor dysfunctions in cerebellar degeneration, Brain 140 (2017) 707–720, https://doi.org/10.1093/brain/aww327.
[53] A.H. Fischer, K.A. Jacobson, J. Rose, R. Zeller, Hematoxylin and eosin staining of tissue and cell sections, pdb.prot4986, CSH Protoc. 2008 (2008), https://doi.org/10.1101/pdb.prot4986.
[54] D. Komura, A. Kawabe, K. Fukuta, K. Sano, T. Umezaki, H. Koda, R. Suzuki, K. Tominaga, M. Ochi, H. Konishi, et al., Universal encoding of pan-cancer histology by deep texture representations, Cell Rep. 38 (2022), 110424, https://doi.org/10.1016/j.celrep.2022.110424.
[55] S.M. Yamada, Y. Tomita, S. Shibui, T. Kurokawa, Y. Baba, A case of breast cancer brain metastasis with a 16-year time interval without evidence of cancer recurrence, J. Breast Cancer 20 (2017) 212–216, https://doi.org/10.4048/jbc.2017.20.2.212.
[56] C. Segnani, C. Ippolito, L. Antonioli, C. Pellegrini, C. Blandizzi, A. Dolfi, N. Bernardini, Histochemical detection of collagen fibers by sirius red/fast green is more sensitive than van gieson or sirius red alone in normal and inflamed rat colon, PLoS One 10 (2015), e0144630, https://doi.org/10.1371/journal.pone.0144630.
[57] E. Roda, E.C. Priori, D. Ratto, F. De Luca, C. Di Iorio, P. Angelone, C.A. Locatelli, A. Desiderio, L. Goppa, E. Savino, et al., Neuroprotective metabolites of hericium erinaceus promote neuro-healthy aging, Int. J. Mol. Sci. 22 (2021) 6379, https://doi.org/10.3390/ijms22126379.
[58] S. Krajewski, A.D. Thor, S.M. Edgerton, D.H. Moore, M. Krajewska, J.C. Reed, Analysis of bax and Bcl-2 expression in P53-immunopositive breast cancers, Clin. Cancer Res. 3 (1997) 199–208.
[59] S.E. Bodrug, C. Aimé-Sempé, T. Sato, S. Krajewski, M. Hanada, J.C. Reed, Biochemical and functional comparisons of Mcl-1 and Bcl-2 proteins: evidence for a novel mechanism of regulating Bcl-2 family protein function, Cell Death Differ. 2 (1995) 173–182.
[60] Z.N. Oltval, C.L. Milliman, S.J. Korsmeyer, Bcl-2 heterodimerizes in vivo with a conserved homolog, bax, that accelerates programed cell death, Cell 74 (1993) 609–619, https://doi.org/10.1016/0092-8674(93)90509-O.
[61] T.P. Berke, S.H. Slight, S.M. Hyder, Role of reactivating mutant P53 protein in suppressing growth and metastasis of triple-negative breast cancer, Onco Targets Ther. 15 (2022) 23–30, https://doi.org/10.2147/OTT.S342292.
[62] P. Li, L. Zhou, T. Zhao, X. Liu, P. Zhang, Y. Liu, X. Zheng, Q. Li, Caspase-9: structure, mechanisms and clinical application, Oncotarget 8 (2017) 23996–24008, https://doi.org/10.18632/oncotarget.15098.
[63] J.L.Y. Chee, S. Saidin, D.P. Lane, S.M. Leong, J.E. Noll, P.M. Neilsen, Y.T. Phua, H. Gabra, T.M. Lim, Wild-type and mutant P53 mediate cisplatin resistance through interaction and inhibition of active caspase-9, Cell Cycle 12 (2013) 278–288, https://doi.org/10.4161/cc.23054.
[64] X. Pu, S.J. Storr, Y. Zhang, E.A. Rakha, A.R. Green, I.O. Ellis, S.G. Martin, Caspase-3 and caspase-8 expression in breast cancer: caspase-3 is associated with survival, Apoptosis 22 (2017) 357–368, https://doi.org/10.1007/s10495-016-1323-5.
[65] L.M. Vargas-Roig, M.A. Fanelli, L.A. López, F.E. Gago, O. Tello, J.C. Aznar, D. R. Ciocca, Heat shock proteins and cell proliferation in human breast cancer biopsy samples, Cancer Detect. Prev. 21 (1997) 441–451.
[66] J.M. Murphy, P.E. Czabotar, J.M. Hildebrand, I.S. Lucet, J.-G. Zhang, S. Alvarez-Diaz, R. Lewis, N. Lalaoui, D. Metcalf, A.I. Webb, et al., The pseudokinase MLKL mediates necroptosis via a molecular switch mechanism, Immunity 39 (2013) 443–453, https://doi.org/10.1016/j.immuni.2013.06.018.
[67] Z. Albakova, G.A. Armeev, L.M. Kanevskiy, E.I. Kovalenko, A.M. Sapozhnikov, HSP70 multi-functionality in cancer, Cells 9 (2020), E587, https://doi.org/10.3390/cells9030587.
[68] L. Gaiaschi, E. Roda, C. Favaron, F. Gola, E. Gabano, M. Ravera, P. Rossi, M. G. Bottone, The power of a novel combined anticancer therapy: challenge and opportunity of micotherapy in the treatment of glioblastoma multiforme, Biomed. Pharmacother. 155 (2022), 113729, https://doi.org/10.1016/j.biopha.2022.113729.
[69] D. Ratto, F. Corana, B. Mannucci, E.C. Priori, F. Cobelli, E. Roda, B. Ferrari, A. Occhinegro, C. Di Iorio, F. De Luca, et al., Hericium erinaceus improves recognition memory and induces hippocampal and cerebellar neurogenesis in frail mice during aging, Nutrients 11 (2019), E715, https://doi.org/10.3390/nu11040715.
[70] Godwin Avwioro Histochemical Uses of Haematoxylin. Journal of Physics; Conference Series 2011, 1, 24–34.
[71] A. Kádár, G. Wittmann, Z. Liposits, C. Fekete, Improved method for combination of immunocytochemistry and nissl staining, J. Neurosci. Methods 184 (2009) 115–118, https://doi.org/10.1016/j.jneumeth.2009.07.010.
[72] E. Roda, S. Barni, A. Milzani, I. Dalle-Donne, G. Colombo, T. Coccini, Single silver nanoparticle instillation induced early and persisting moderate cortical damage in rat kidneys, Int. J. Mol. Sci. 18 (2017), E2115, https://doi.org/10.3390/ijms18102115.
[73] R. Lattouf, R. Younes, D. Lutomski, N. Naaman, G. Godeau, K. Senni, S. Changotade, Picrosirius red staining, J. Histochem. Cytochem. 62 (2014) 751–758, https://doi.org/10.1369/0022155414545787.